MANIPULATING PLASTICITY THROUGH CONTROL OF COLLOIDAL INTERACTIONS

BY

ANDRES CADAVID

A THESIS
SUBMITTED TO THE FACULTY OF

ALFRED UNIVERSITY

IN PARTIAL FULFILLMENT OF THE REQUIREMENTS
FOR THE DEGREE OF

MASTER OF SCIENCE

IN

CERAMIC ENGINEERING

ALFRED, NEW YORK

DECEMBER, 2004

MANIPULATING PLASTICITY THROUGH CONTROL OF COLLOIDAL INTERACTIONS

BY

ANDRES CADAVID

B.S. UNIVERSIDAD EAFIT (2001)

SIGNATURE OF AUTHOR (Signature on file)

APPROVED BY (Signature on file)
WILLIAM CARTY, ADVISOR

(Signature on file)
HARRIE STEVENS, ADVISORY COMMITTEE

(Signature on file)
WALTER SCHULZE, ADVISORY COMMITTEE

(Signature on file)
DOREEN EDWARDS, CHAIR, ORAL THESIS DEFENSE

ACCEPTED BY (Signature on file)
ALASTAIR CORMACK, DEAN,
SCHOOL OF ENGINEERING

ACKNOWLEDGMENTS

I would like to thank Dr. William Carty for his guidance through this research. His help made possible the accomplishment of this project. I would also like to thank my advisory committee, Dr. Harrie Stevens and Dr. Walter Schulze, for their valuable comments to improve my work and their effort to help me finish my thesis on time.

I am thankful to the Corona Organization for giving me the opportunity for my professional development. Special thanks to Gabriel Arango and Juan Antonio Montoya for making this experience possible. I thank everyone in Gamma for their support and help, especially David Mesa, Carlos Humberto Zapata and all the people in the technical department.

This work would not have been possible without the help of Hyojin Lee, Ungsoo Kim, Brett Schulz, Brian Pinto, David Finkelnburg, Jon Mccann, Thomas Lam, Eric Nichols, Brian Tanico, and everyone else in the Whiteware Research Center from which I learned many valuable things that not only allowed me to complete this project, but will be extremely helpful in my life. Special thanks to Emily Freeman and Jeanette Harris for their assistance.

I would like to thank all the technical specialists for their help with the instruments and equipment used, specially Terry Guild

Very special thanks to my friend Felipe Mejia who encouraged me to work hard to complete this project and helped me overcome many difficulties. Thanks to all my friends in Alfred for making the stay here more enjoyable. I want to specially thank my father, my mother, my brother, and all my family and friends in Colombia who always supported me and made the experience of being away from home a lot easier.

TABLE OF CONTENTS

LIST OF TABLES

LIST OF FIGURES

ABSTRACT

Green and fired properties of three electrical porcelain bodies were compared. The three bodies were not significantly different, except for their plasticity. One of the bodies required a higher water content to develop similar plastic characteristics (27 %d.w.b. compared to 21 and 22%d.w.b.). To modify the plasticity of this body, changes in the particle size distribution of the coarse particles and modifications in particle-particle interactions were evaluated. Plasticity was not affected by changes in particle size distribution of the coarse particles made by replacement of coarser feldspars for the regular feldspar. Particle-particle interactions, in turn, showed a significant effect on the plasticity of the body. Plasticity was manipulated by dispersant and coagulant additions. Reductions in the water content required for extrusion from 27 %d.w.b. to as low as 20.4 %d.w.b were achieved by the addition of dispersant.

I. INTRODUCTION

Drying cracks, forming problems, and machining difficulties are issues in the manufacturing of commercial porcelain that have always been attributed to poor plasticity of the body. Plasticity can be defined as the ability of a material to be permanently deformed without rupture. Because of their small size and plate-like shape, clay minerals provide plasticity in a porcelain body.

Historically, plasticity has been difficult to characterize. However, the development of new techniques to measure plasticity of porcelain bodies make it possible to better understand this important property.

In this study, an electrical porcelain body was compared with other commercial electrical porcelain bodies to identify properties of the body which could be improved. Based on this comparison, it was felt that the plasticity of the body under study could be improved. It was proposed that by adjusting dispersant and coagulant additions, the plasticity of the body under study can be optimized and controlled in such a way that it is less affected by raw material variations. The improvement of plasticity allows for extrusion at lower water contents, which reduces shrinkage and the possibilities for cracking.

Water content, particle size and particle size distribution, and particle-particle interactions are the most important factors that influence plasticity. Increasing water content, while it improves plasticity of the body, has the disadvantage of increasing shrinkage. With an increase in shrinkage, there are greater chances of cracking. The modification of particle-particle interactions is done by adding dispersants or coagulants to the body. The particle size and particle size distribution of the body are limited by the ingredients in the batch. The amount and particle size of economically available raw materials to a great extent dictate the particle size and particle size distribution of the body. Fired properties often dictate the amount of each raw material required, so adjustments to any batch composition are limited within a narrow range. The particle size and particle size distribution becomes dependent on variations in raw materials, and to counteract them, limited changes in the batch composition are possible.

A. Background and Literature Review

1. Clay Minerals

The basic components of a porcelain body are clay, feldspar, and quartz. A typical porcelain batch contains around 45% of clay, and because of its high specific surface area, it accounts for around 95% of the surface area of the batch, making it a decisive component in the rheology and plasticity of the body.[1]

One of the most important components of clays is kaolinite, a 1:1 sheet silicate were a tetrahedral layer of $[Si_2O_5]^{-2}$ and an octahedral layer of $[Al_2(OH)_4]^{+2}$ are coupled together.[2] Kaolinite is formed by the weathering of feldspars and muscovite present in rocks such as granites and rhyolites. The weathering process leaches out potassium and silica. If potassium is not leached completely, illite results. Clays can be found on residual, hydrothermal, and sedimentary deposits. The residual and hydrothermal deposits are considered primary, i.e. the weathering process occurred in the place where the deposit is found. Sedimentary deposits are considered secondary, i.e. the weathering products were transported and deposited in a different place.[3]

2. Properties of Clay Suspensions

The fine particle size and plate-like shape of kaolinite give clays their characteristic plastic behavior when mixed with water. Rheological and plastic properties of clay suspensions depend on particle-particle interactions, particle concentration, particle size and distribution, particle shape, and the rheology of the suspending medium.[4]

Polyelectrolytes and counterions modify particle-particle interactions. They act as dispersants and coagulants respectively. In the case of dispersants, repulsive forces between particles are promoted, creating a deflocculated suspension with low viscosity. Coagulants reduce repulsive forces between particles, promoting agglomeration.[5] It has been shown that at a neutral pH, the hexagonal plate-like particles of kaolinite have the silica-like plane surface negatively charged, and the aluminum hydroxide-like plane surface positively charged, so the adsorption of dispersants takes place on the alumina-like plane and the edge instead of the traditional belief that it takes place only on the edges.[2]

It has been shown that rheology and plasticity of a batch depends on the ionic strength of the medium.[6,7] At a low concentration of divalent cations, a deflocculated state is promoted. When the divalent cation concentration is increased over the critical coagulation concentration, the suspension viscosity increases significantly and the cohesion stress of the plastic body is reduced.[8] The coagulated state is promoted by compression of the double layer; specific adsorption of the counterion is unnecessary.

The cations affecting the rheology and plasticity of a body come from direct additions of coagulants or from dissolution from the clay minerals. Sillapachai determined that the concentration of divalent cations dissolved from clay suspensions depends on the specific surface area of raw materials, the quantity of monovalent cations present, mixing time and intensity, and aging time.[9]

Plastic forming is used to manufacture porcelain insulators. Processes like extrusion and hot pressing are used to give the shape to a ceramic insulator. The behavior of the body on the forming process depends on its rheological and plastic characteristics.

3. Rheology and Plasticity

Rheology is the study of flow or deformation of substances. Viscosity is a measure of the resistance of a fluid to flow. The viscosity of Newtonian fluids is independent of shear rate. Non-Newtonian fluids exhibit a more complicated behavior because their viscosity depends on shear rate; this is the case of suspensions used in ceramic processes. The viscosity of pseudoplastic fluids decreases with increasing shear rate, i.e, they present shear thinning behavior. Dilatant fluids have shear thickening characteristics. Thixotropy, which is the decrease in viscosity with time at a constant shear rate, is another phenomenon common in clay-based suspensions.[4]

Because of the morphology of clay particles, clay suspensions have particular rheological characteristics depending on the state of flocculation. When a flocculated suspension is at rest, the attractive forces bring particles together and a three-dimensional network forms. When this suspension is sheared, an initial force is required to break the network, with a yield stress associated with this process. As shear increases, the network continues to be broken into smaller flocs, so the viscosity at higher shear rates is

lower.[4,10] With time, particles align in the direction of flow, so the resistance to flow is reduced, and the viscosity decreases.[4]

Understanding plasticity is fundamental to process control, but plasticity is a difficult property to characterize.[11] Several tests have been developed to measure plasticity. The Atterberg plasticity test is used to determine the plastic limit and liquid limit of a material. The plastic limit is the moisture content at which the material stops behaving plastically and becomes fragile. The liquid limit is the moisture content at which the material starts acting as a fluid. The Pfefferkorn plasticity test is used to measure the most suitable moisture content for shaping.[12] Baran *et al.* applied a method used to determine the workability of metals to measure the plasticity of clays. They used data from compression and upset testing of cylindrical samples of different moisture content to determine the workability of clays.[12] Many tests used to measure plasticity are performed at low pressure or in an unconfined state, so the results may not correlate very well with real processes.

To measure the plasticity of ceramic systems under pressures similar to those found in real processes, the HPASC rheometer is used. In this device, the shear rate and the applied pressure are controlled. The measured variable is shear stress. With the applied pressure and the shear stress, the cohesion and pressure dependence of the sample are calculated. These define the plasticity of the sample.[11]

4. The Principle of Effective Stress Applied to Plasticity Characterization

The most important principle of soil mechanics that can be successfully applied to plasticity of clay-based materials is that of effective stress. If an external stress is applied to a clay-water mixture, the stress is distributed between the particle network and the water phase. The stress acting on the particle network is the effective stress, and the stress supported by the water is the pore water pressure. The stress distribution between the two depends on the kind of stresses and the relative concentration of water and solids. The particle network and the pore water can share normal stresses, but shear stresses can only be supported by particles.[13]

The principle of effective stress states that strains in a body are only caused because of the effective stress and not because of the total stress. For example, when a hydrostatic stress is applied to a body that is saturated with water, all the pressure is

contained by the pore water, i.e. the effective stress is zero. No compaction takes place. On the other hand, if an isostatic stress is applied to a dry body, all the stress is effective stress. This means that the particle network deforms and compacts.

5. Raw Material Variations

When chemical and mineralogical variations occur in raw materials, the processing properties and product characteristics are altered. Hahn compared the effects of a kaolin of variable quality and a kaolin of stable properties on the finished product and working properties of a porcelain body. He concludes that even in bodies with small percentages of kaolin, the working and body properties are seriously affected by variations in the properties of this raw material.[14]

Caughel developed a simple method to detect clay variability by segregation through gravity sedimentation. By documenting the volume and appearance of distinct layers of sediment of a clay suspension, variations between batches of clay can be detected.[15]

II. EXPERIMENTAL PROCEDURE

The body under study was identified as Body 2. Body 1 and Body 3 were the commercial electrical porcelain bodies used for comparison. The chemical composition of the bodies is shown in Table I. The location of the bodies in the Silica-Leucite-Mullite sub-diagram is shown in Appendix C. Samples of the three bodies were received in the plastic state. For the determination of general properties, samples were dried at 110°C overnight and crushed using a mortar and pestle. For the determination of fired properties, rods were extruded in a vacuum pug mill (Rawdon Limited, Burton on Trent, England).

Table I. Chemical Composition of the Bodies in Weight Percent.

BODY	SIO_2	AL_2O_3	FE_2O_3	MGO	CAO	NA_2O	K_2O	TIO_2
1	65.68	26.68	0.56	0.15	0.35	1.12	4.62	0.72
2	**72.20**	**20.68**	**0.89**	**0.19**	**0.22**	**1.63**	**3.37**	**0.72**
3	72.81	19.66	0.61	0.17	0.34	1.00	4.52	0.78

A. General Properties

Basic properties such as particle size distribution (PSD), density, specific surface area (SSA), chemical composition, and loss on ignition (LOI) were measured. Particle Size Distribution was measured in the SediGraph 5100 (Micromeritics, Norcross, GA). Suspensions for PSD determination were prepared at 30 v/o, dispersed with Na-PAA (Darvan 811) and ultrasonicated for 10 minutes. Density was determined in a Helium pycnometer (Accupyc 1330, Micromeritics, Norcross, GA). Before measuring the density, samples were dried at 110°C overnight and allowed to cool to room temperature in a desiccator.

For the SSA determination, the multipoint BET (Brunauer-Emmett-Teller) method was used in a Gemini Surface Area Analyzer (Micromeritics, Norcross, GA). Before measuring the SSA, approximately 1.0 g of each sample was outgassed at 150°C with flowing N_2 for one hour and allowed to cool before analyzing.

The chemical composition of the samples was obtained by ICP-AES (Induction Coupled Plasma – Atomic Emission Spectroscopy, ACME Laboratories Ltd., Vancouver, British Columbia, Canada). To compare the chemical composition of the bodies, the results were converted to Unity Molecular Formula (UMF). Standard methods were used to determine LOI.[16]

B. Firing of Samples

Since the optimum firing temperature for Bodies 1 and 3 was not known and expected to be different from Body 2, the comparison of firing properties was done as a function of firing temperature. To narrow the temperatures at which the bodies were to be fired, determination of a firing range common to all samples was done with a gradient furnace. Samples of approximately 20 mm long were cut from extruded rods of each body. The diameter of each specimen was measured along a scribed line so the diameter after firing could be measured along the same direction again. Samples were loaded in the gradient furnace spaced one inch starting from a reference point in the tube. The gradient furnace was heated at a rate of 104 K/h (1.7°C/min). The peak temperature was held for three hours. After two hours of dwell, the temperature profile inside the tube was measured at one inch intervals starting from the reference point where the first sample was loaded. Several firings were done increasing the peak temperature each time. This procedure was repeated for each of the three bodies until enough data was collected to have specimens fired in a wide range of temperatures covering from underfiring to overfiring conditions.

Fired samples were measured to determine firing shrinkage and used to determine bulk density and apparent porosity according to ASTM standard C20-00.[17] The results are shown in Figure 1, Figure 2, and Figure 3. It can be seen that the three bodies present maximum shrinkage and density and minimum apparent porosity in the range from 1210°C to 1275°C. This was the firing range chosen to fire the samples for the comparison of fired properties.

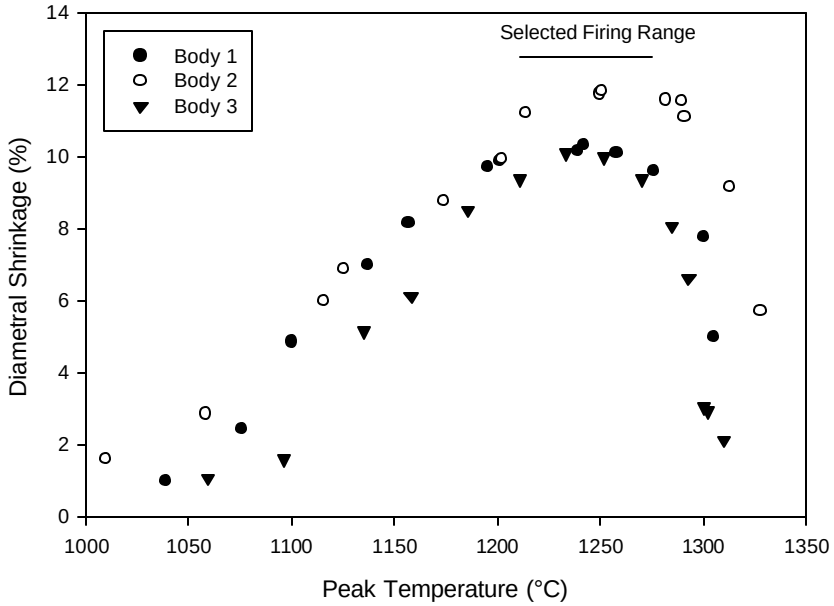

Figure 1. Shrinkage of the samples fired in the gradient furnace.

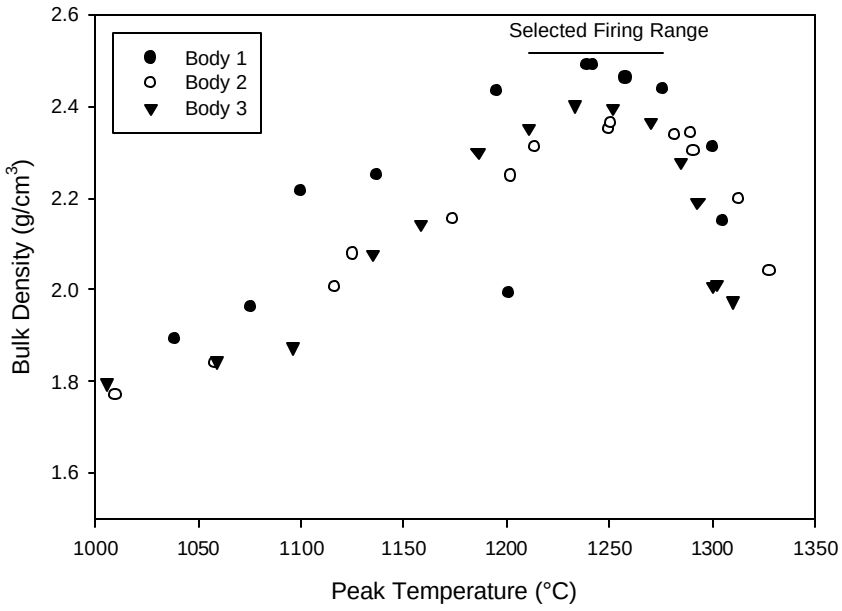

Figure 2. Bulk density of the samples fired in the gradient furnace.

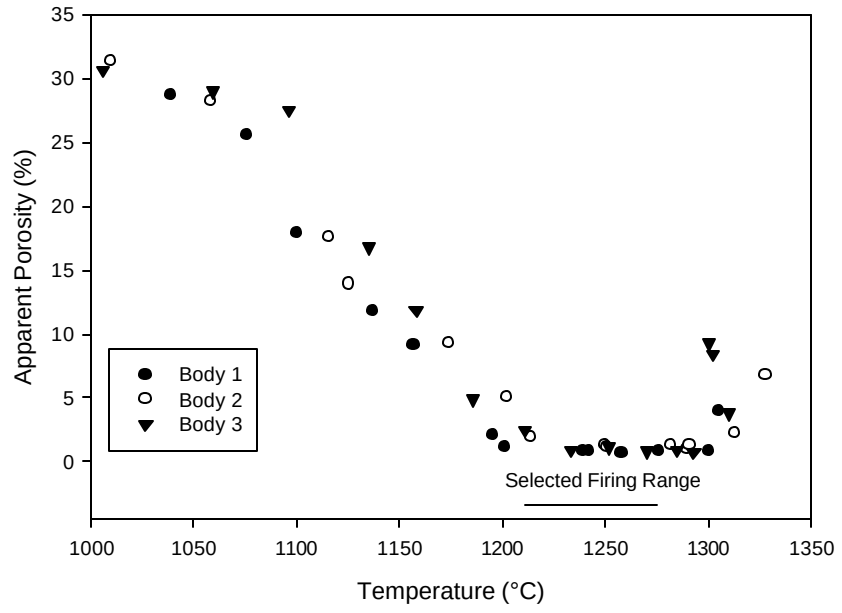

Figure 3. Apparent porosity of the samples fired in the gradient furnace.

After determining the firing range, samples were fired in the roller hearth kiln (Alfred University, Alfred, NY). The peak temperatures chosen were 1210, 1225, 1240, 1260, and 1275°C. Twenty rods of each body were fired at a given temperature randomly distributed in three setters. Rods were fired horizontally on a layer of tabular alumina to avoid sticking to the setters. Orton Tempcheks were used as independent means for measuring the peak temperature.

C. Firing Shrinkage and Bulk Density

Rods were used to determine firing shrinkage. Length and diameter were measured for 25 rods of each body before firing. Five of these rods were fired at each temperature and their fired dimensions determined in the same way as they were measured before firing.

Pieces from the rods were used for the determination of bulk density. The procedure in ASTM standard C20-00 was used.[17]

D. Strain in the Quartz Particles

Strain in the quartz particles was determined via X-ray diffraction to measure the shift in the (112) peak of quartz using a procedure modified from Pinto.[18] To measure the real strain in the quartz crystals, no grinding or polishing could be done to the samples. The D-500 diffractometer (Siemens, Germany) was used because of its benefits of better precision and sample spinning capabilities. The sampler holders used in this diffractometer can only fit a disc-shaped sample of 24.9 mm in diameter and 1.2 mm in thickness. A special sample preparation procedure was necessary. Rods of ¾ of an inch in diameter were extruded and dried. Thin slices were cut from the dry rods in a low speed saw. The optimum thickness was found to be 1.27 mm. This gave a disc thick enough to withstand cutting and thin enough to fit in the sample holder after firing. The average fired diameter of the discs was 18 mm. This gave a big enough area to be irradiated by the incident X-ray beam in this instrument.

A special way to fire the discs was necessary so they wouldn't warp. Discs were fired between two dry pressed porcelain tiles. Between the tiles and the discs, a flat, uniform layer of alumina was used to prevent sticking.

A layer of Apiezon Q was used to mount each disc in the sample holder. The disc was pressed with a glass slide, so it was aligned with the border of the sample holder. On top of the disc, a very thin layer of silicon standard was applied with a paint brush. Silicon standard was used to calibrate peak positions on the XRD pattern, so sample displacement effects were minimized. XRD patterns were collected from 19 to 57° 2θ using a step of 0.02° 2θ and a count time of 30 seconds. The resulting pattern had three silicon peaks that were used to calibrate the position of all peaks in the diffraction pattern.

The quartz peak around 50° 2θ corresponding to the (112) spacing was used for the calculation of strain. To obtain the d-spacing of unstrained quartz crystals, an unfired disc was used, and the same procedure for sample mounting and XRD data collection was followed.

E. Phase Composition

Quantitative x-ray diffraction (QXRD) was used to determine the amount of crystalline phases present in the different bodies. Powder samples were obtained by grinding pieces from rods in a mortar and pestle. 0.300 grams of an internal standard (fluorite) were mixed with 2.700 grams of each sample using a vibratory dry mixer. XRD patterns were acquired in the D500 (Siemens, Germany) from 19 to 57° 2θ using a step of 0.04° 2θ and a count time of four seconds. Three peaks for each phase were used for the calculations. The peaks used are listed in Table II. Each peak was profile fitted in Jade version 6.0 (Materials Data, Inc., Livermore, CA, 2002) and its area used in the calculation to obtain the phase composition. For the calculation, the sum of the areas of the three peaks of each phase was divided by the sum of the areas of the fluorite peaks. This ratio was input into the calibration curves for each phase from which the volume percent of each phase was obtained. Volume percent values were then converted to weight percent.

Table II. Location of Peaks Used for QXRD.

Phase	° 2q
Mullite	30.9, 33.2, 40.8
Quartz	20.9, 40.3, 50.1
Corundum	37.8, 43.3, 52.5
Fluorite	28.3, 47.0, 55.7

F. Flexural Strength

Flexural strength was determined on unglazed rods extruded using a die with an opening of 1.5 cm in diameter. Twenty rods were tested for each body at each firing temperature. A 3-point bending test was used, in which the span was set to 90 mm, and a loading rate of 0.5 mm/min was used. The instrument used for the test was an Instron model 8562 (Instron Corp., Canton, MA). After testing, the diameter of each rod at the failure area was determined and used for the calculation of flexural strength, using the equation:

$$s = \frac{8PL}{pd^3} \qquad (1)$$

Where s is the flexural strength, P is the load at failure, L is the span, and d is the diameter of each rod.

G. Plasticity Characterization

Plastic characteristics, i.e. cohesion and pressure dependence, were measured for each body using the HPASC rheometer for a range in water content from ~10% dry weight basis (d.w.b.) to ~30% d.w.b. in ~2% increments.

The procedure commonly used to prepare the samples for the HPASC is outlined by Kupinski.[19] In this procedure, the dry sample is mixed in a torque rheometer cell (Model# BEO6-00175, C.W. Brabender, So. Hackensack, NJ), and distilled water is added up to the desired water content. In the manufacturing of electrical insulators, batches are prepared by dispersing the raw materials in water. Dispersion in water gives

better mixing results than dry mixing.[20] Because the objective of the present study was to characterize the plasticity of the bodies as they are used in the manufacturing process, a different procedure was required to obtain the samples. In the new procedure developed, the water content of each plastic body was increased to 30% d.w.b. and then slowly dried to the desired water content.

Preliminary tests in the Brabender showed that for a sample with water content of 30% d.w.b., 450 grams was an adequate amount to be mixed properly. Water content in the original bodies was determined from the weight loss of a portion of sample dried at 110°C overnight. The amount of original sample and additional water required to have 450 g of sample with a water content of 30% d.w.b. were calculated. The corresponding amount of each original sample was mixed with the additional distilled water in the brabender for 15 minutes. Then, the sample was removed from the brabender, loaded again and mixed for 15 additional minutes to guarantee uniformity in the water content.

Plasticity determinations were done at water contents ranging from 10% d.w.b. to 28% d.w.b. At each level of water content, 100 grams of sample were loaded to the HPASC. Each 100g-sample was obtained by drying from the 30% d.w.b. batch an amount calculated using the equation:

$$w = 100 \times \frac{(100+30)}{(100+x)} \qquad (2)$$

Where w is the amount of batch required, and x is the desired water content for the plasticity measurement in percent d.w.b.

This amount of sample (w) was shaped into a ball and allowed to dry at room temperature in a controlled fashion with the aid of a fan to move the air around the samples. Drying of the samples was monitored by weight. When each sample reached 100 grams, it was stored in a plastic bag and tested in the HPASC as soon as possible. The water content of each sample after testing in the HPASC was determined and used for the plasticity plots.

Non uniform drying of the sample was avoided by drying at room temperature and shaping the sample as a ball. This way, thin areas or edges which might dry unevenly were avoided. Room temperature made drying slower and allowed for better control.

Before each sample was tested in the HPASC, it was shredded and loaded to the sample cell. The cell was mounted in the instrument and rotated for four minutes to allow for escape of air in the sample. After that time, the air vent was shut and the test started. For testing, the rotation speed was fixed at 0.5 RPM. Data was collected every three seconds for two minutes at each pressure. The values of applied pressure were 550, 740, 920, 1130, and 1310 kPa. The resulting plots of shear stress versus pressure applied to the sample were fitted with a linear equation from which the values of pressure dependence (slope) and cohesion (intercept) were obtained. An example of this plot is found in Figure 4.

In addition to the characterization of plasticity in the HPASC, plastic limit determinations were also done. To determine the plastic limit of samples, ASTM standard D 4318-00 was used.[21]

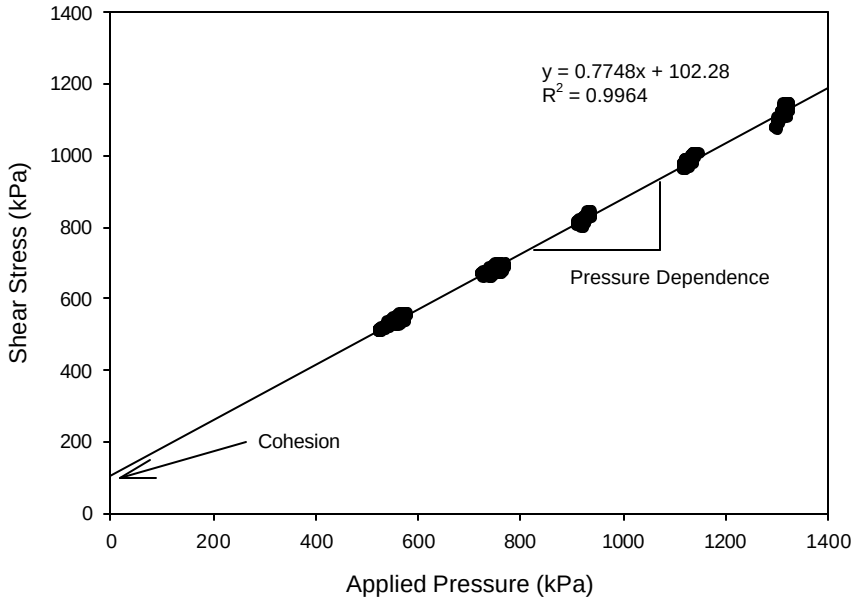

Figure 4. Example of a plot obtained from the HPASC data.

H. Effect of Particle Size Distribution on the Plasticity of the Body under Study

Two series of bodies were batched in which the regular feldspar was replaced by coarser feldspars. In the first series, a feldspar of the same characteristics as the regular feldspar was obtained from the supplier with modifications in the particle size distribution. This feldspar was ground to a coarser particle size distribution. In the

second series, G200 feldspar was used. The particle size distributions of the feldspars used are compared with the regular feldspar in Figure 5.

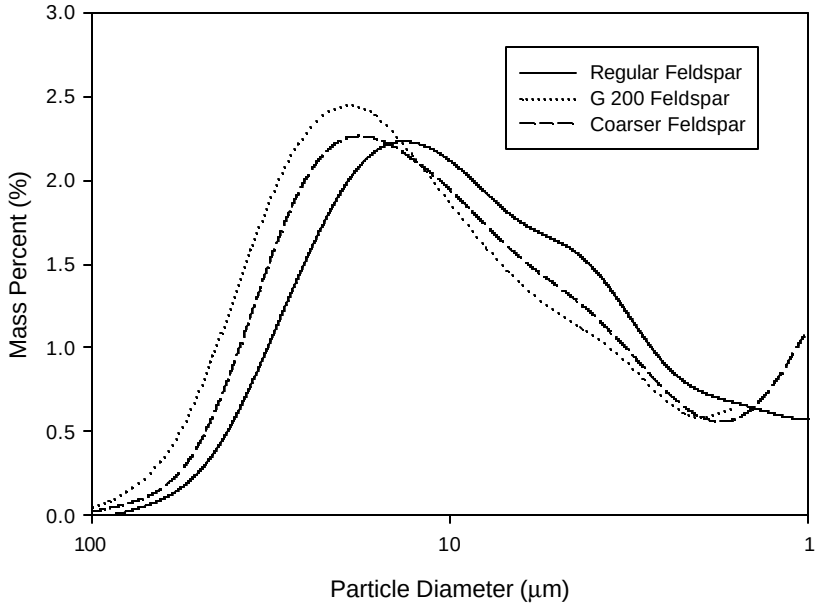

Figure 5. Particle size distribution of the feldspars used.

The body was batched using the same formula used in the manufacturing process. One five-liter suspension with the regular feldspar, one 2.5-liter suspension with the coarser feldspar, and one 2.5-liter suspension with G200 were batched. Each suspension was batched at a solids loading of 33v/o, and mixed thoroughly.

Because of the lower purity of the regular feldspar, the suspension batched with G200 required an adjustment of the feldspar level so the body had the same silica and flux levels as originally formulated. This was done by mixing the G200 with quartz in a ratio that the levels of SiO_2 and fluxes remained equal to the original formulation of the body.

0.8-liter suspensions were made by blending each endpoint. The resulting composition of the batches is shown in Table III.

Table III. Batches of the Series Changing Feldspar in Body 2.

SERIES	BATCH CODE	FELDSPAR COMPOSITION IN BATCH
Regular – Coarse	C 0	100% regular feldspar
Regular – Coarse	C 25	75% regular feldspar, 25% coarser feldspar
Regular – Coarse	C 50	50% regular feldspar, 50% coarser feldspar
Regular – Coarse	C75	25% regular feldspar, 75% coarser feldspar
Regular - Coarse	C100	0% regular feldspar, 100% coarser feldspar
Regular – G200	G 0	100% regular feldspar
Regular – G200	G 25	75% regular feldspar, 25% G200 mix feldspar
Regular – G200	G 50	50% regular feldspar, 50% G200 mix feldspar
Regular – G200	G75	25% regular feldspar, 75% G200 mix feldspar
Regular – G200	G100	0% regular feldspar, 100% G200 mix feldspar

Each 0.8-liter suspension was shaken overnight in the shaker bath, mixed in the high intensity disperser for 20 minutes, and then filterpressed in baroid filters. The resulting cakes of each batch were mixed in the brabender. From each batch, samples for the HPASC were prepared to be tested at three water contents. From these three samples, the general shape of the plasticity curves could be assessed. Plastic limit was also measured for each batch.

I. Effect of Dispersant Additions on the Plasticity of the Body under Study

A preliminary study was done to determine the proper amount of dispersant to be added. The dry body was dispersed in DI water with different dispersant levels. The dispersant used was Na-PAA (Darvan 811). Each sample was shaken overnight in the shaker bath. After shaking, the apparent viscosity of each sample was determined using a stress-controlled rheometer (AR2000, TA instruments, New Castle, DE). Then, each sample was filterpressed, and its plasticity determined in the HPASC at a water content of 19±0.5% d.w.b. The plastic limit was also determined for these samples.

Viscosity as a function of dispersant level is shown in Figure 6. Points C and D correspond to the amount of dispersant needed to reach minimum viscosity. These were chosen for further evaluation of the effect of dispersant on plasticity. These points correspond to dispersant levels of 0.05 and 0.1 mg/m^2. Plasticity as a function of dispersant addition is shown in Figure 7.

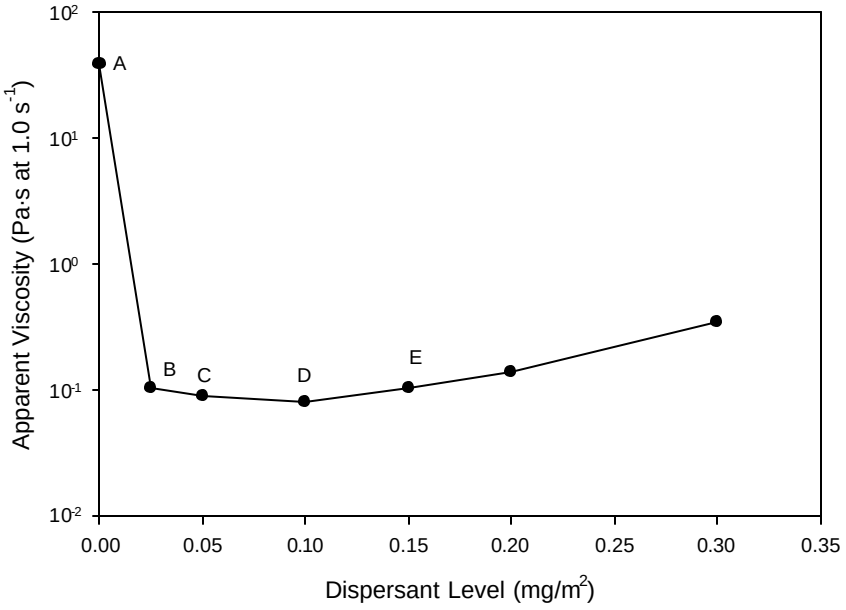

Figure 6. Viscosity as a function of dispersant added.

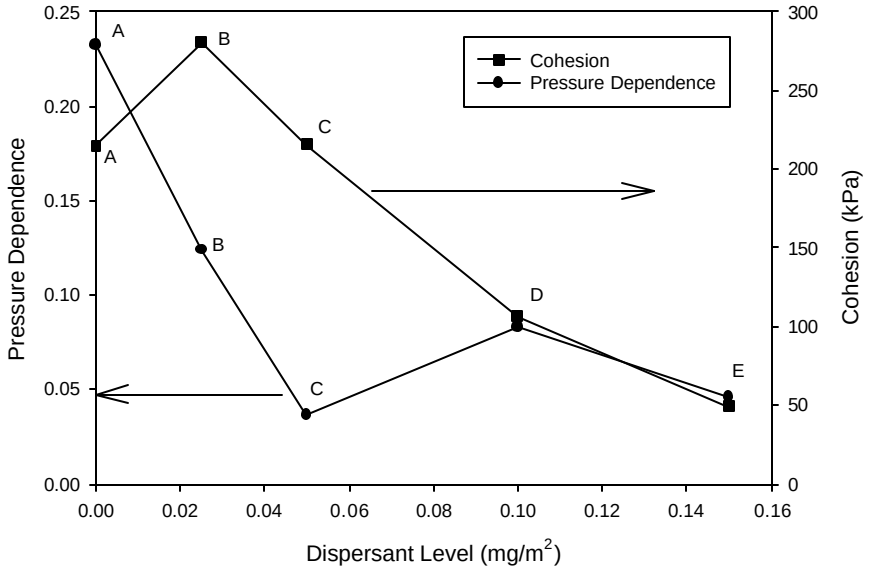

Figure 7. Plasticity versus dispersant level.

To determine the effect of dispersant on the complete plasticity curves, 0.8-liter suspensions of the body with 0.05 and 0.1 mg/m^2 dispersant were prepared, thoroughly mixed, shaken overnight, and filterpressed to obtain cakes. Cakes for each sample were mixed in the brabender and samples for the HPASC were obtained in the same way as explained before.

J. Effect of Coagulant Additions on the Plasticity of the Body under Study

Another set of 0.8-liter suspensions of the body with 0.05 and 0.1 mg/m^2 dispersant were prepared. Before filterpressing, the samples were coagulated adding $CaCl_2$ to reach a 10 mM [Ca^{+2}].

III. RESULTS AND DISCUSSION

A. General Properties

The results from the determination of basic properties like density, LOI, and SSA are shown in Table IV. The three bodies have similar properties. Body 1 has a higher density attributed to the presence of corundum. Body 2 has higher SSA.

Table IV. Basic Green Properties.

Body	Density (g/cm^3)	LOI (%)	SSA (m^2/g)
1	2.67 ± 0.01	4.9 ± 0.01	11.49 ± 0.05
2	**2.62 ± 0.01**	**5.0 ± 0.01**	**13.55 ± 0.05**
3	2.62 ± 0.01	4.8 ± 0.01	11.79 ± 0.05

The particle size distribution analysis is shown in Figure 8. While Body 1 and Body 3 have similar particle size distributions, the PSD of Body 2 is different. The main difference is in the coarse particles range. The left side of the PSD curve of Body 2 is shifted to the right. This means that the coarse particles in Body 2 are finer than the coarse particles in the other bodies.

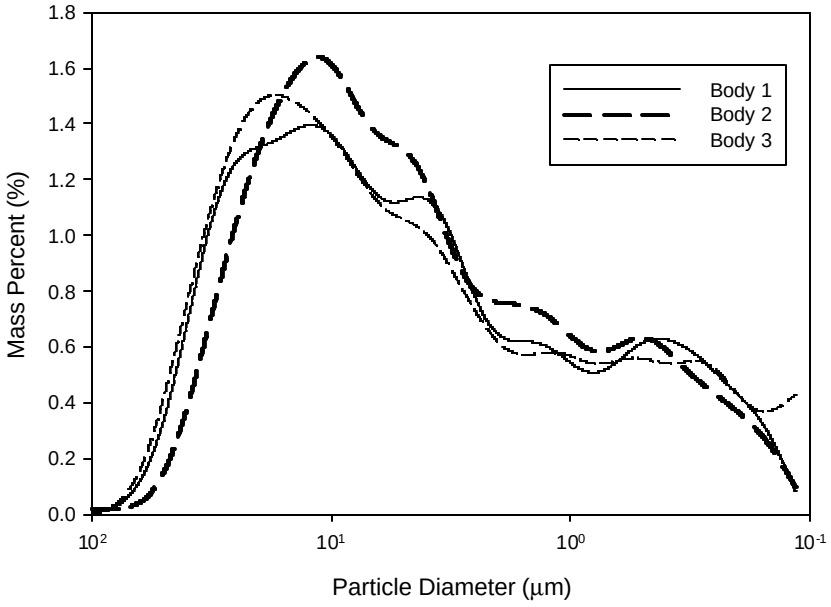

Figure 8. Particle size distribution of the bodies.

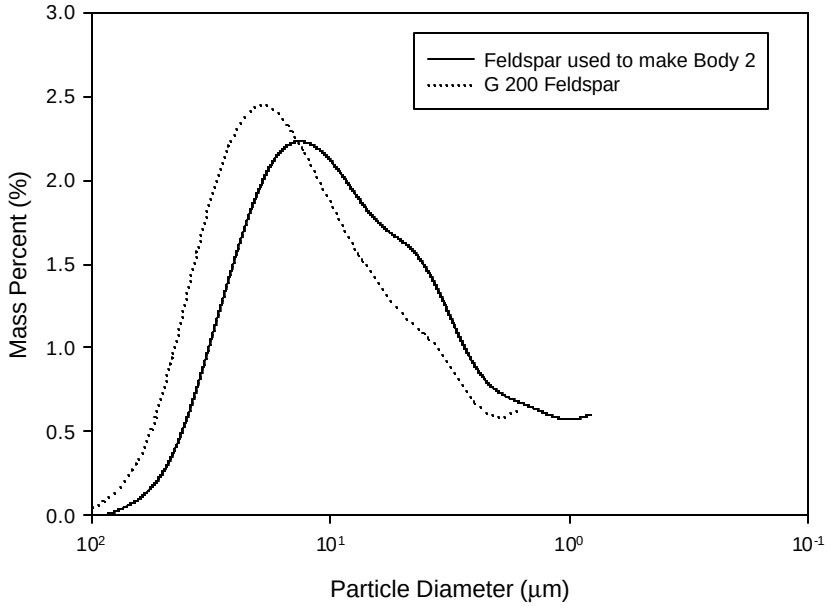

Figure 9. Particle size distribution of the feldspar used to make Body 2 compared to G200.

In Figure 9, the PSD of the feldspar used to make Body 2 is compared with the PSD of G200, which is a feldspar commonly used in the industry. The coarser side of the

PSD of the feldspar used to make Body 2 is also shifted to the right when compared to G200. The difference in the coarser fraction of the PSD of the bodies can be explained by the different PSD of the feldspar used.

The chemical composition in UMF of the three bodies is shown in Table V. The three bodies have similar chemical composition. Body 1 has higher alumina content. Again, this is attributed to the presence of corundum. The ratio of potash to soda is slightly lower in Body 2.

Table V. Chemical Composition of the Bodies in UMF.

BODY	**SIO_2**	**AL_2O_3**	**FE_2O_3**	**MGO**	**CAO**	**NA_2O**	**K_2O**	**TIO_2**
1	14.17	3.39	0.05	0.05	0.08	0.23	0.64	0.12
2	**16.94**	**2.86**	**0.08**	**0.07**	**0.06**	**0.37**	**0.50**	**0.13**
3	16.32	2.60	0.05	0.06	0.08	0.22	0.65	0.13

B. Firing of Samples

A typical temperature profile for the firing in the roller kiln is shown in Figure 10. The temperature values plotted in this figure were obtained from the thermocouples located in the kiln crown. In this kiln, peak temperature is automatically controlled at point A. Measured values at A are very close to the set point. Temperature control at B required manual adjustments of the electrical heating elements.

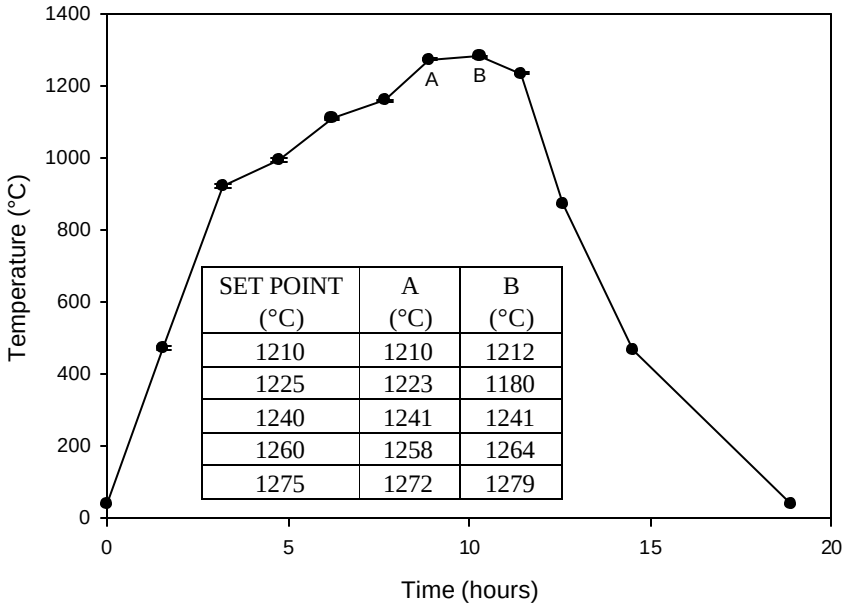

SET POINT (°C)	A (°C)	B (°C)
1210	1210	1212
1225	1223	1180
1240	1241	1241
1260	1258	1264
1275	1272	1279

Figure 10. Typical firing profile for the roller hearth kiln. Points A and B indicate the peak temperatures for each set point.

The peak temperature data from the tempcheks is shown in Figure 11. There is a difference between the setpoint and the temperature values reached in the kiln. Because of this, peak temperature values from the tempcheks were used for the plots of fired properties.

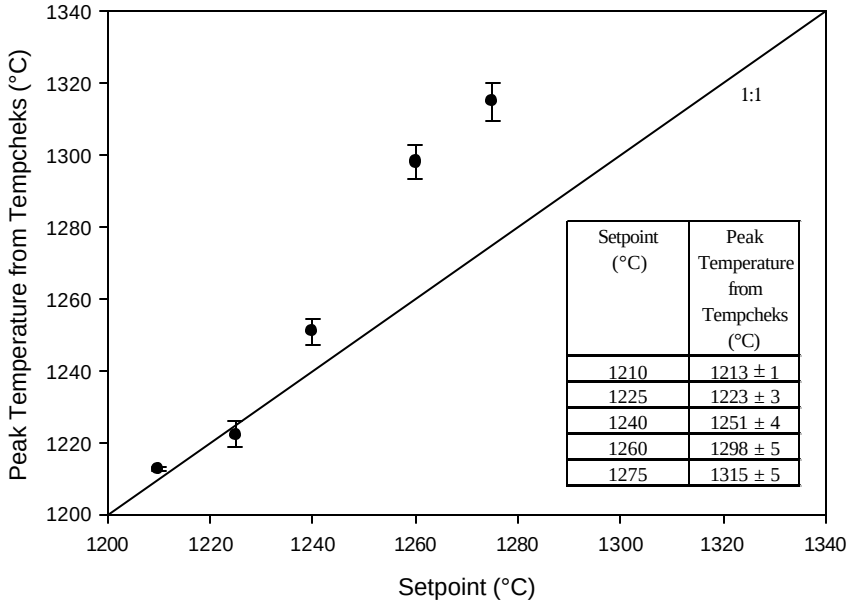

Setpoint (°C)	Peak Temperature from Tempcheks (°C)
1210	1213 ± 1
1225	1223 ± 3
1240	1251 ± 4
1260	1298 ± 5
1275	1315 ± 5

Figure 11. Peak temperature data from tempcheks.

C. Firing Shrinkage and Bulk Density

Shrinkage results are shown in Figure 12. Body 2 has higher firing shrinkage than the other bodies. This can be a consequence of the higher water content required for plastic formation of Body 2 because a less compact structure is formed during drying.

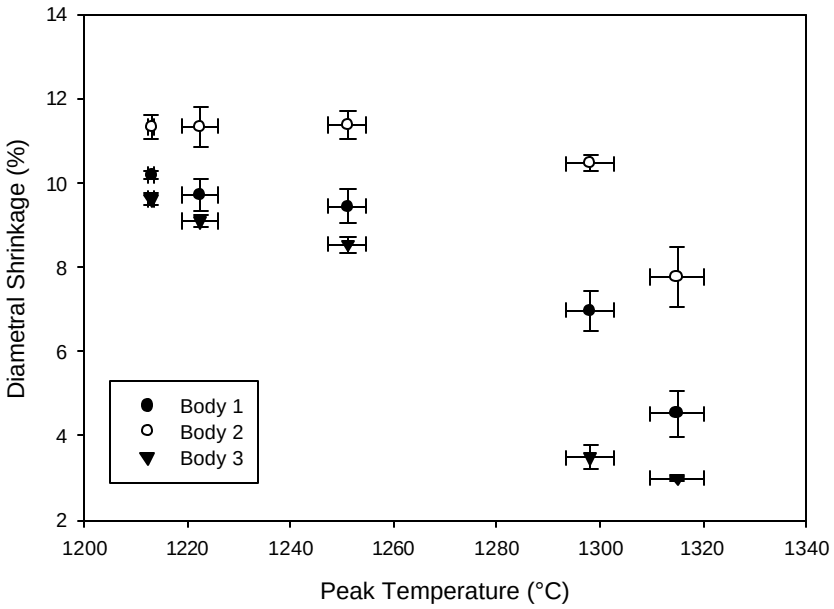

Figure 12. Firing shrinkage of the bodies as a function of firing temperature.

Bulk density is shown in Figure 13. Similar to the green density data, Body 1 has higher fired bulk density attributed to the presence of corundum. To analyze the effect of temperature on the bodies, shrinkage and bulk density data was normalized. To do so, every point was divided by the maximum value of each body. The results are shown in Figure 14 and Figure 15. It can be seen that Body 2 has a broader firing range that the two other bodies.

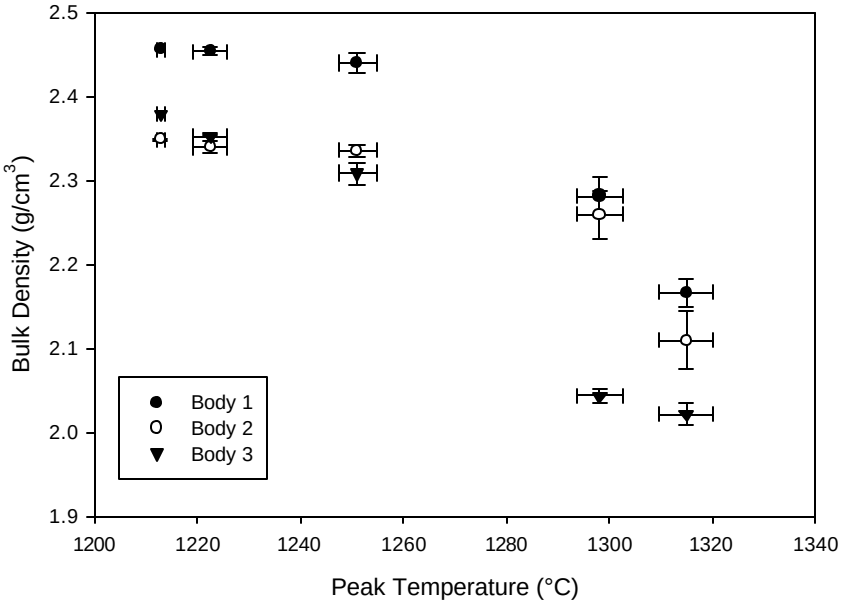

Figure 13. Bulk density of the bodies as a function of firing temperature.

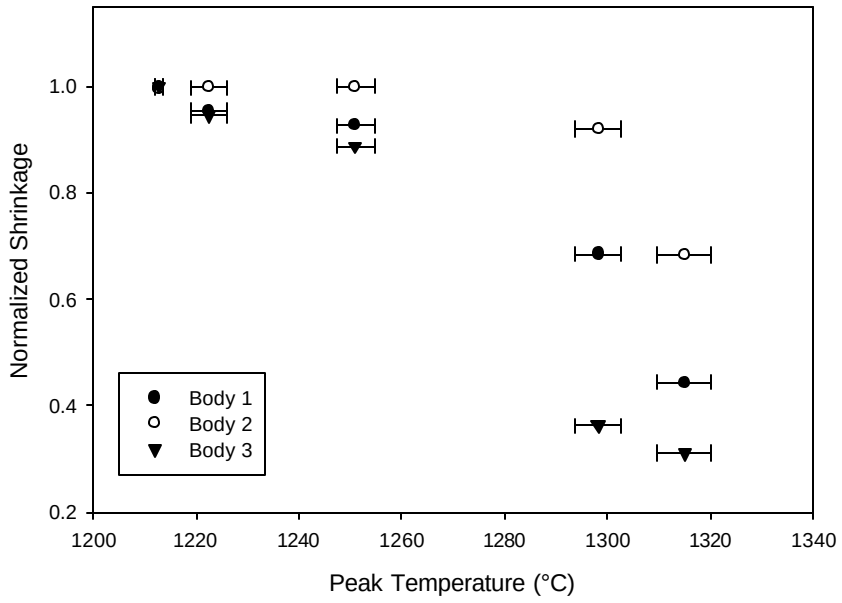

Figure 14. Normalized shrinkage of the bodies as a function of firing temperature.

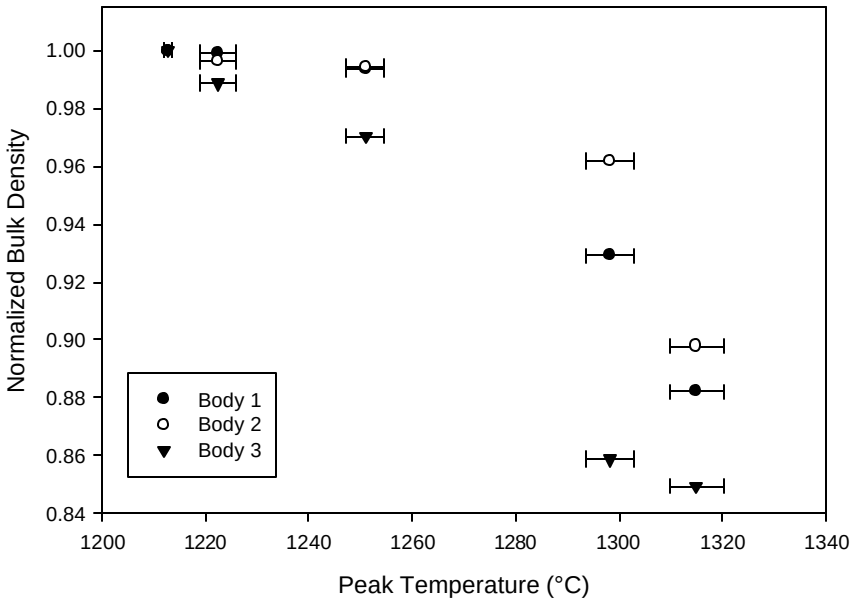

Figure 15. Normalized bulk density for the three bodies as a function of firing temperature.

D. Strain in Quartz Particles

Measured d-spacing in the [112] direction for quartz particles is shown in Table VI. The difference in values is within 0.001 Å, which is within the standard deviation estimated from the profile fit, so there is no effect of temperature or body on the d-spacing of quartz particles in this direction.

Table VI. d-spacing and Strain in the [112] Direction for Quartz.

Peak Temperature (°C)	**d-spacing (Å)**			**Strain**		
	Body 1	**Body 2**	**Body 3**	**Body 1**	**Body 2**	**Body 3**
1213	1.828	1.829	1.828	0.005	0.006	0.005
1223	1.829	1.829	1.829	0.006	0.006	0.006
1251	1.828	1.829	1.829	0.005	0.006	0.006
1298	1.829	1.830	1.829	0.006	0.006	0.006

With these values, the average strain in the quartz particles was calculated using an equilibrium d-spacing of 1.8183 Å obtained from measurements of unfired discs. The average value of strain in the quartz particles is 0.006±0.0003.

The average strain value was used to calculate the quartz particle size using the relationship between strain and particle size found by Pinto,[18] which is shown in Figure 16. The calculated particle size in the fired bodies is 38.3±0.6 µm.

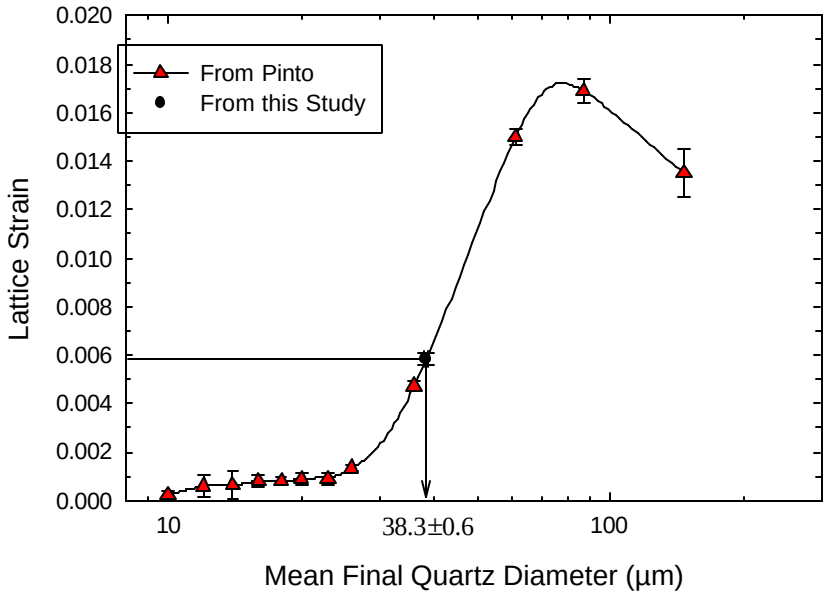

Figure 16. Strain as a function of quartz particle size. Modified from Pinto.[18]

E. Phase Composition

Results from QXRD analyses are shown in Figure 17, Figure 18, and Figure 19. Body 3 has some corundum, believed to come from process contamination. Body 1 shows a significant amount of corundum (around 10%), which seems too high to be caused by contaminations. Body 2 has no corundum. Because of increased solubility of silica in the glass phase, quartz concentration decreased with increasing temperature.

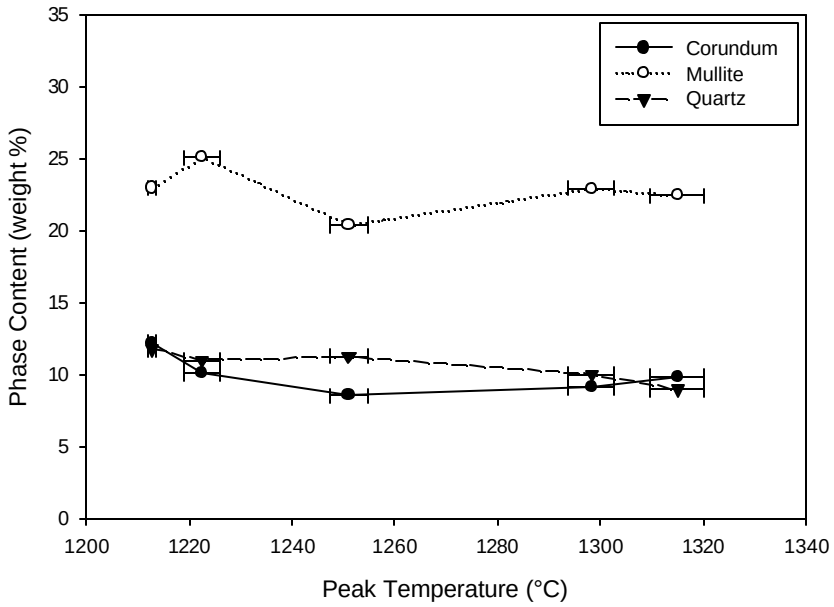

Figure 17. Concentration of crystalline phases in Body 1 as a function of firing temperature.

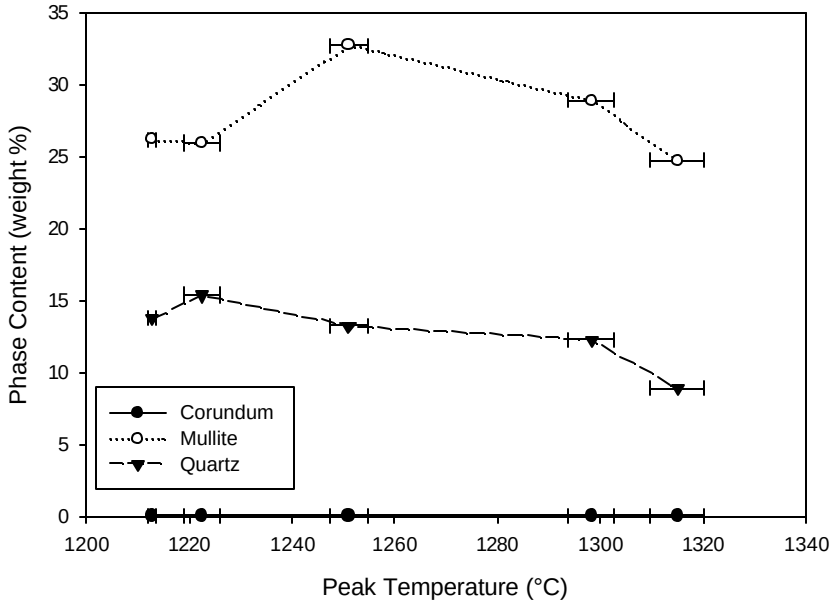

Figure 18. Concentration of crystalline phases in Body 2 as a function of firing temperature.

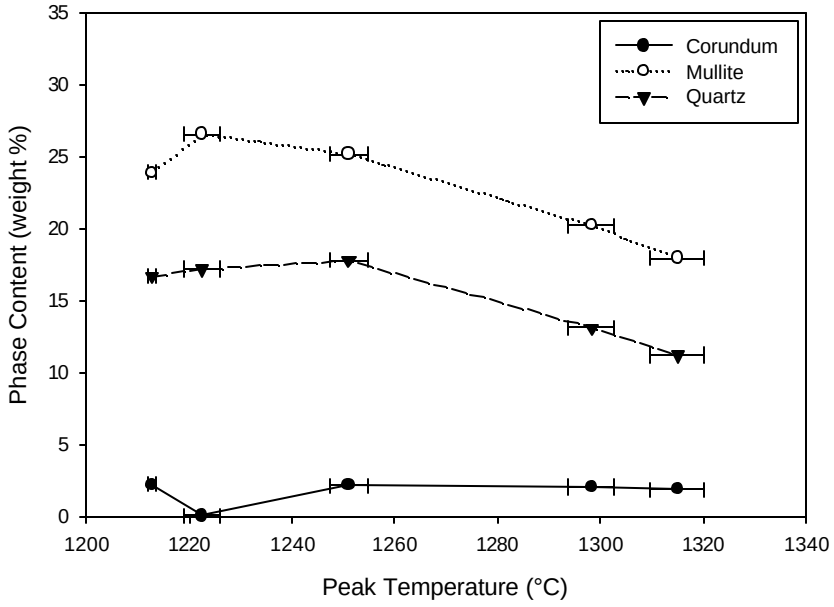

Figure 19. Concentration of crystalline phases in Body 3 as a function of firing temperature.

F. Flexural Strength

Flexural strength results of the three bodies are plotted as a function of temperature in Figure 20. The strength of the three bodies is very similar; the effect of firing temperature is the same as for shrinkage and bulk density. Body 1, even with ~10% corundum, has flexural strength similar to Body 2. Body 2 has shown its superiority in terms of fired properties. Its high flexural strength and broader firing range are advantages over the other bodies.

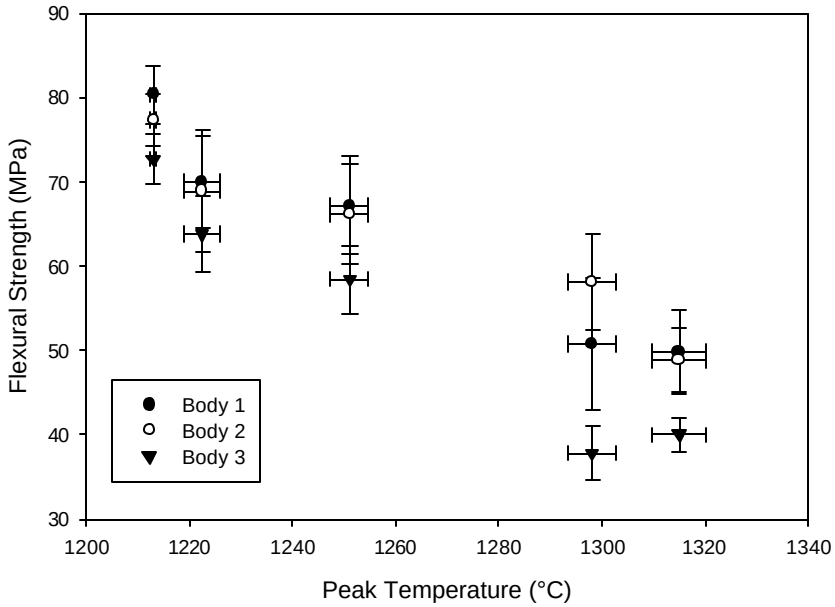

Figure 20. Flexural strength of the bodies as a function of firing temperature.

G. Plasticity Characterization

The results of plasticity measurements for the three bodies are shown in Figure 21 and Figure 22. Error bars indicate one standard deviation, and they were calculated using results from a repeatability study previously done by Lee.[22] Body 1 and Body 3 are somewhat similar in behavior. Plasticity curves of Body 2 show a significant difference; they are shifted to higher water content. Body 2 requires more water to attain sufficient plasticity, which contributes to higher shrinkage, increasing the possibilities of cracking during drying and firing.

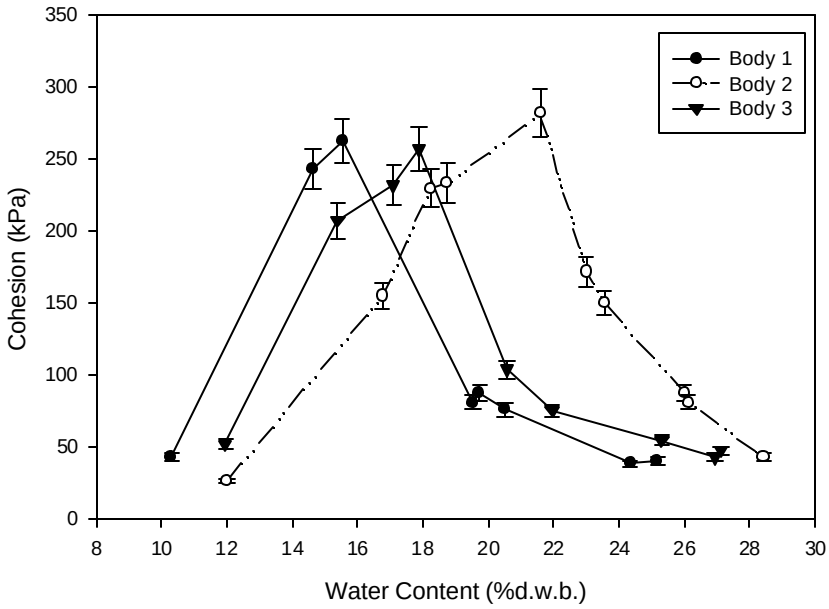

Figure 21. Cohesion versus water content.

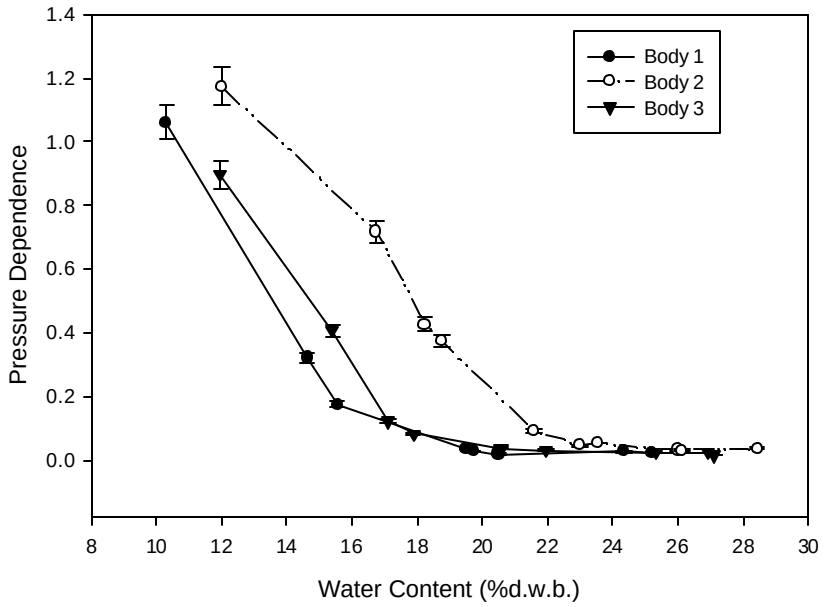

Figure 22. Pressure dependence versus water content.

Data from plastic limit determinations, shown in Table VII, support these results. The plastic limit correlates very well with the plasticity curves. The plastic limit is very close to the water content for the maxima in cohesion and to the point where pressure dependence becomes independent of water content.

Table VII. Plastic Limit for the Bodies Compared.

Body	**Plastic Limit (% d.w.b.)**	**Water Content at Maximum Cohesion Value (% d.w.b.)**	**Break Point on Pressure Dependence Curve (% d.w.b.)**
1	16	16	17
2	**21**	**22**	**23**
3	17	18	18

Water content determinations in the samples as received are shown in Table VIII. They show that Body 2 is used with more water than the other bodies. At the water contents at which the bodies are used, pressure dependence is independent of water

content, and cohesion values for each body are similar. In Figure 23, a detail of the cohesion curve around the as-received water content shows that cohesion values are around 71 ± 4 kPa (67 to 75 kPa). This value seems logical for extrusion compared to 50 kPa which is the strength of the particle network.[23]

Table VIII. Water Content in the Samples as Received.

Body	Water Content as Received (% d.w.b.)
1	21
2	27
3	22

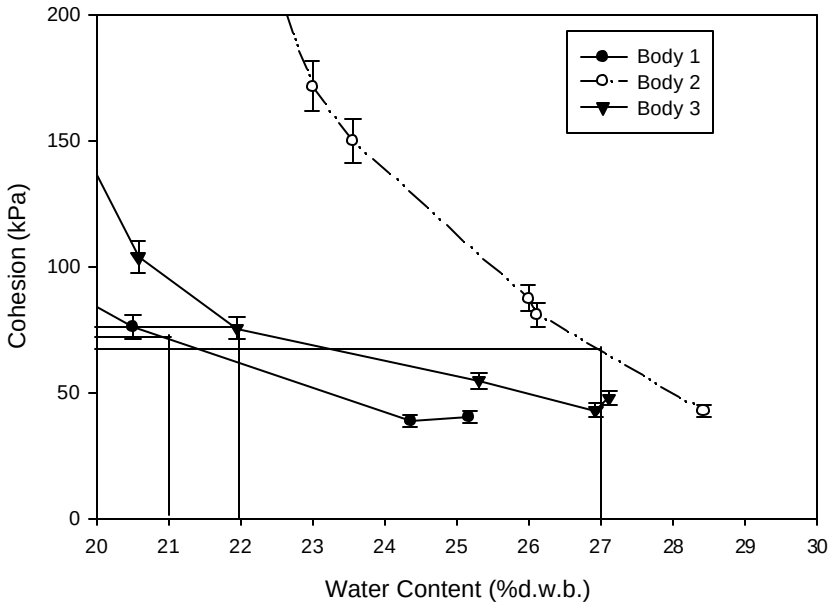

Figure 23. Detail of cohesion for the three bodies around the as-received water content.

If this cohesion interval from 67 to 75 kPa is interpreted as the extrudable range of these bodies, a range of water content for extrusion can be determined. This is shown in Figure 24.

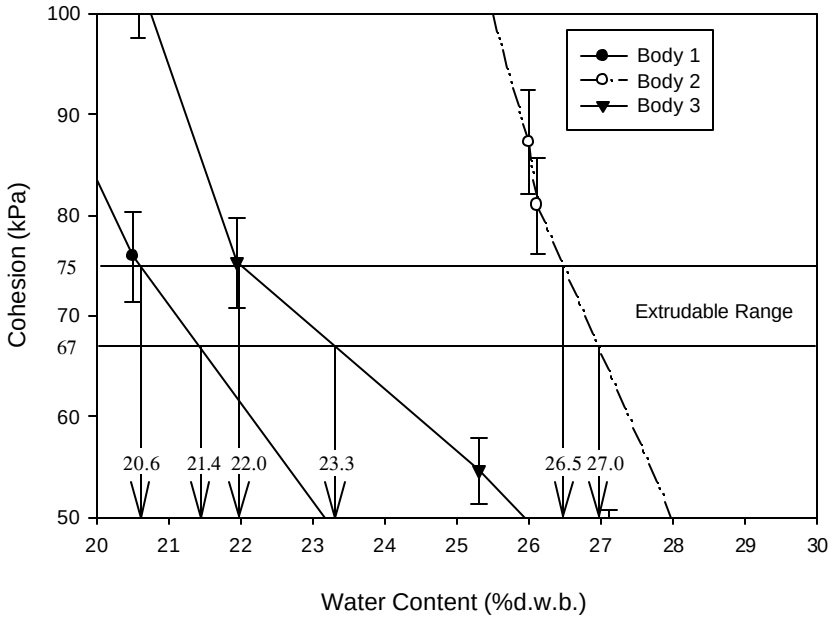

Figure 24. Detail of the extrudable range of the three bodies.

The range of water content for extrusion of the different bodies is shown in Table IX. The range of Body 2 is narrower. Its width is 0.5 % compared to 0.8% and 1.3% for bodies 1 and 2 respectively.

Table IX. Range of Water Content for Extrusion.

Body	**Range of Water Content for Extrusion (% d.w.b.)**
1	20.6 – 21.4
2	26.5 – 27.0
3	22.0 – 23.3

H. Effect of Particle Size Distribution on the Plasticity of the Body under Study.

The PSD of the batches in each series is shown in Figure 25 and Figure 26. As expected, the addition of coarser feldspar shifted the left side of the distribution to coarser levels.

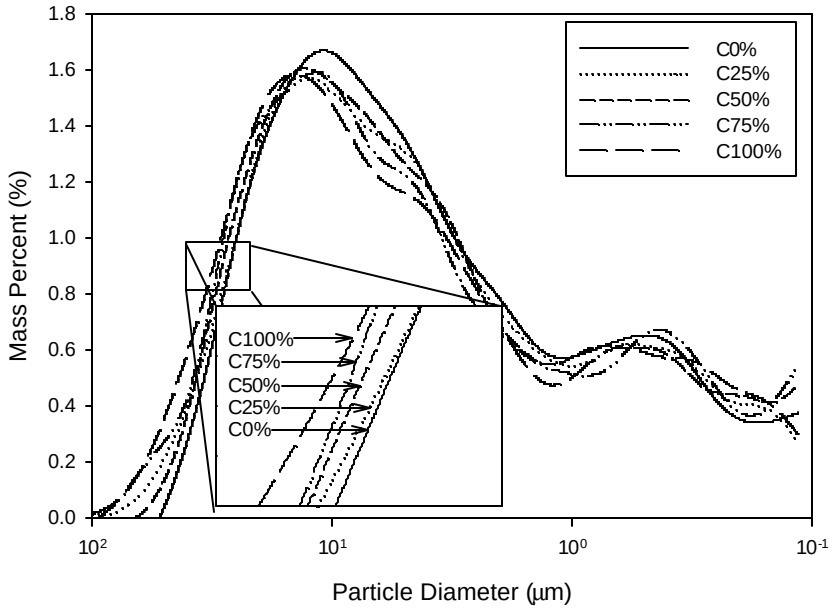

Figure 25. PSD of the series replacing coarser feldspar for regular feldspar.

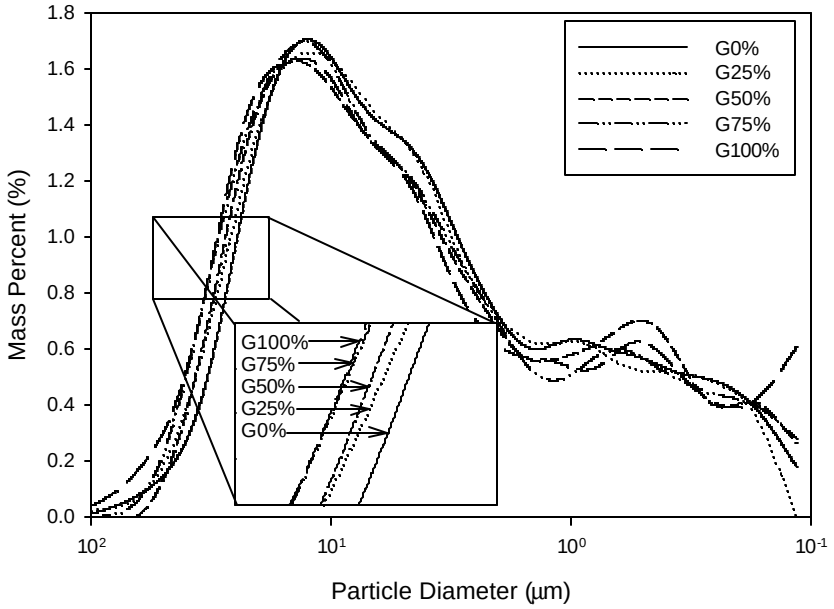

Figure 26. PSD of the series replacing G200 mix for regular feldspar.

In whiteware bodies, although particle size distributions are not optimized for packing, commercial bodies are nonetheless typically well-packed. Whiteware bodies are blends of relatively coarse feldspar, medium sized quartz, finer kaolin, and even finer ball clays. Proportions in the blend have been adjusted over the years to improve properties and performance during plastic forming, drying, and firing. These well packed systems are not very sensitive to changes in PSD, especially in the coarser fractions.[23]

Plasticity curves for the series of feldspar replacement tests are shown in Figure 27 to Figure 30. Regardless of the level of feldspar replacement, all plasticity points for both series are located along plasticity curves very close to the original curve for body 2. This shows that in this system, particle size distribution of the feldspar had no effect on plasticity.

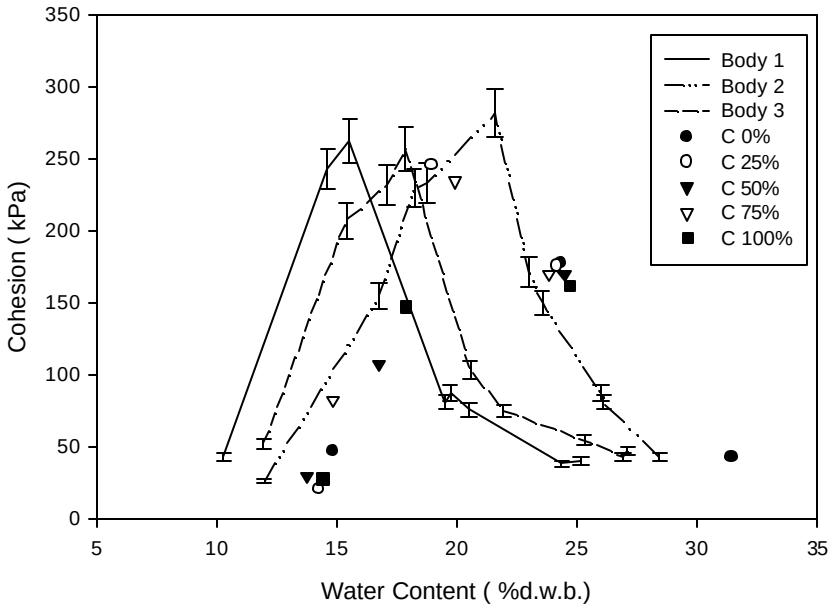

Figure 27. Cohesion versus water content for the series replacing coarser feldspar for regular feldspar. Bodies 1, 2, and 3 are included for reference.

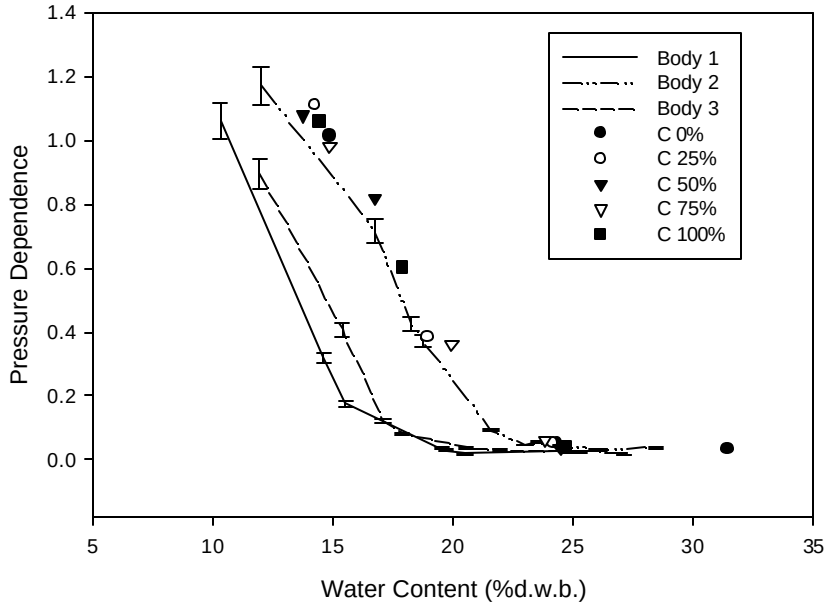

Figure 28. Pressure dependence versus water content for the series replacing coarser feldspar for regular feldspar. Bodies 1, 2, and 3 are included for reference.

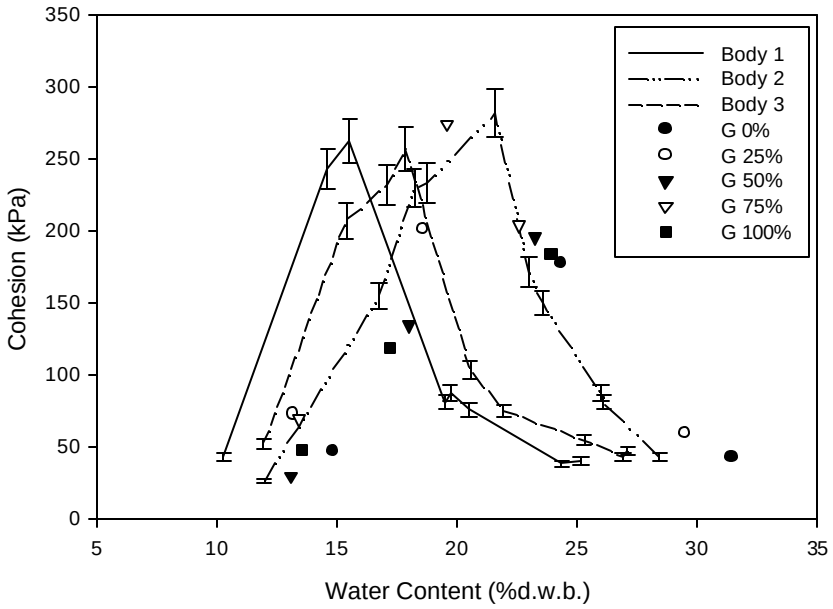

Figure 29. Cohesion versus water content for the series replacing G200 mix for regular feldspar. Bodies 1, 2, and 3 are included for reference.

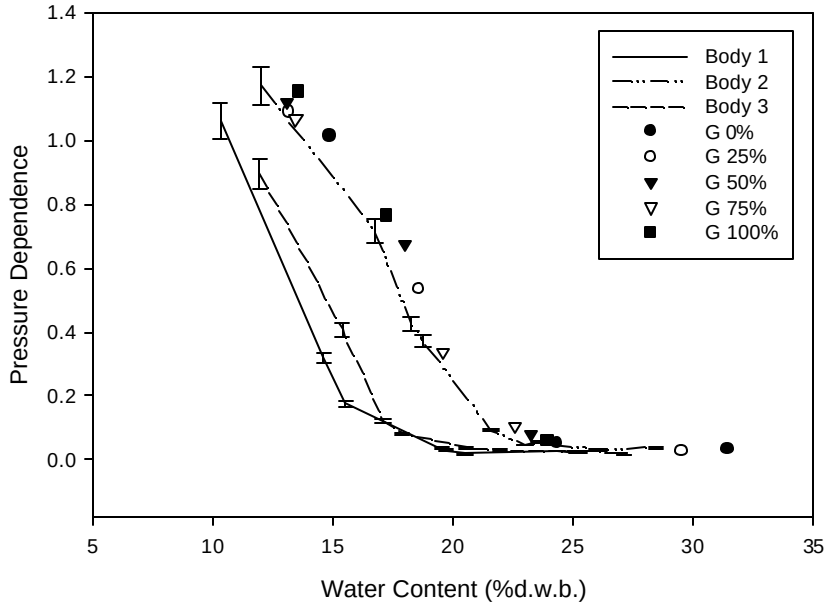

Figure 30. Pressure dependence versus water content for the series replacing G200 mix for regular feldspar. Bodies 1, 2, and 3 are included for reference.

I. Effect of Dispersant Additions on the Plasticity of the Body under Study.

Plasticity results from the preliminary study are shown in Figure 7 and Figure 31. They show that dispersant additions effectively shift the plasticity curve of the body to lower water contents. The decrease in the plastic limit shows that the cohesion peak is moving toward lower water contents.

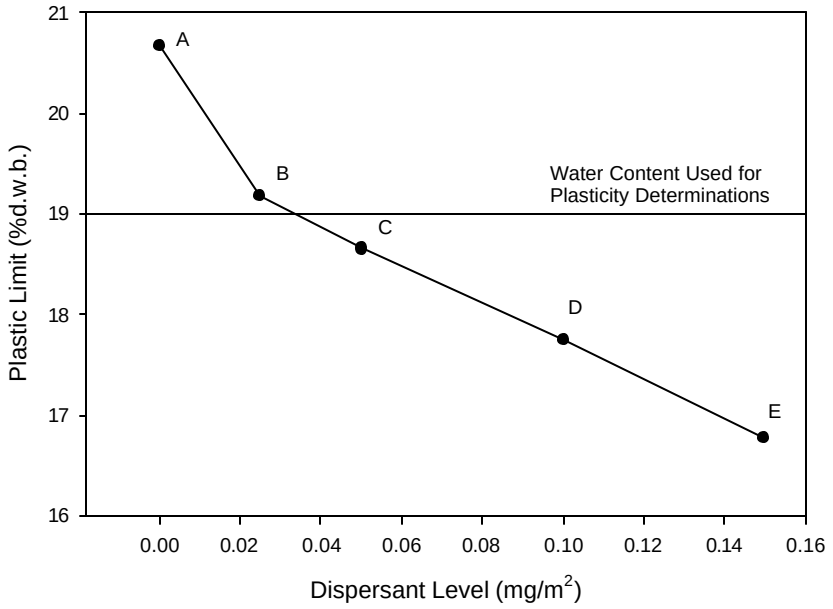

Figure 31. Plastic limit versus dispersant level for the preliminary test.

Cohesion and pressure dependence values support this. When going from A to B, cohesion increases and pressure dependence decreases because the measurement was done at water contents below the plastic limit. From B to E, cohesion decreases and pressure dependence reaches a minimum because they are being measured at water contents above the plastic limit. An illustration explaining this is shown in Figure 32.

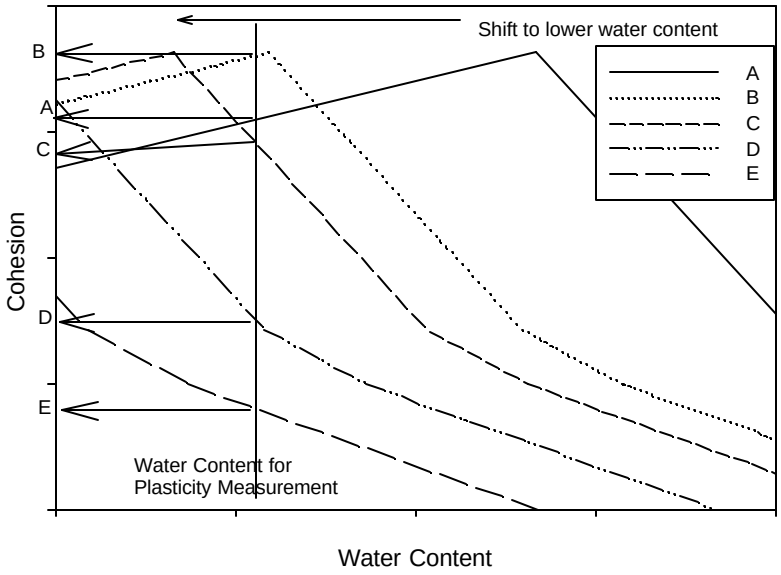

Figure 32. Illustration showing the shift in the cohesion curve.

Results from the complete plasticity test support the results from the preliminary test. Plasticity curves for tests with dispersant levels of 0.05 and 0.1 mg/m^2 and no $CaCl_2$ are shown in Figure 33 and Figure 34. Dispersant additions shift plasticity curves to lower water contents. Kupinski also found that dispersant additions reduced cohesion and pressure dependence.[19] His observations are consistent with the results of the present study. However, the effect of calcium chloride additions on plasticity was not found.

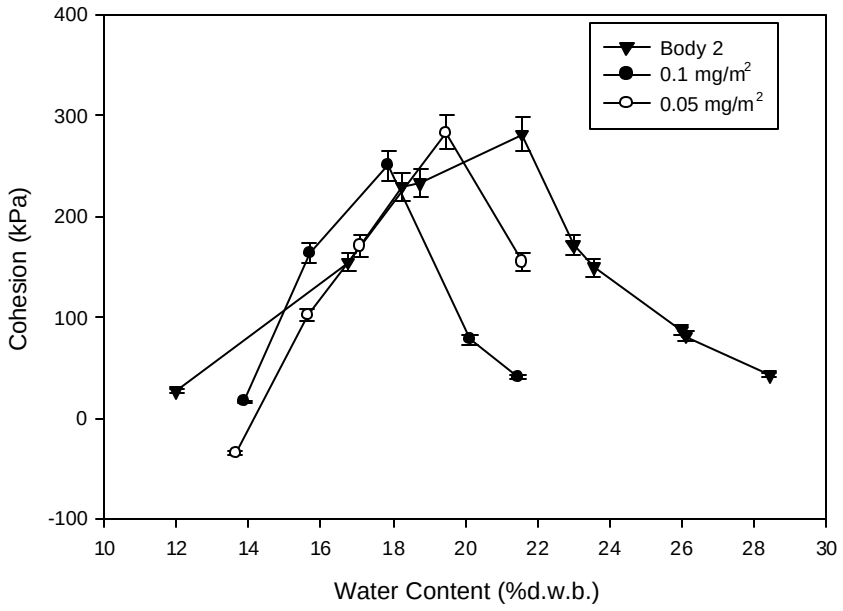

Figure 33. Cohesion versus water content for dispersant additions.

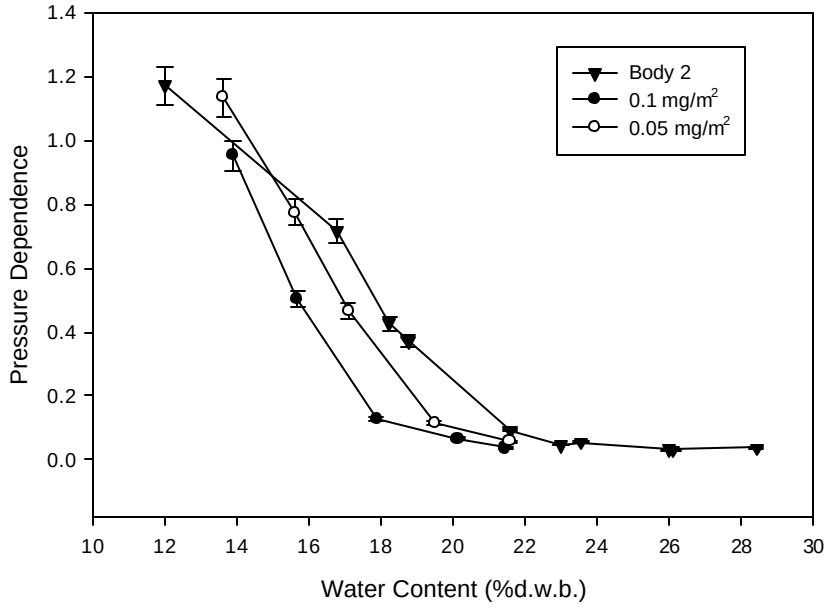

Figure 34. Pressure dependence versus water content for dispersant additions.

The shift to lower water contents is explained by the nature of the dispersed system and soil mechanics. When the system is dispersed, particles pack better. A higher solids content is necessary for particles to touch each other and support an effective stress.[13] In other words, a dispersed system requires lower water content to behave like a flocculated system.

J. Effect of Coagulant Additions on the Plasticity of the Body under Study.

The results from the experiment in which calcium chloride was added to the dispersed batches to coagulate them are shown in Figure 35 and Figure 36. The curve for 0.1 mg/m^2 of dispersant, which without adding $CaCl_2$ was shifted to lower water contents, is now shifted to higher water contents when $CaCl_2$ was added. This is consistent with the previous explanation for the dispersed system. Now that the system is coagulated, an effective stress can be built up at higher water contents because of the poorly packed structure formed by the particles.

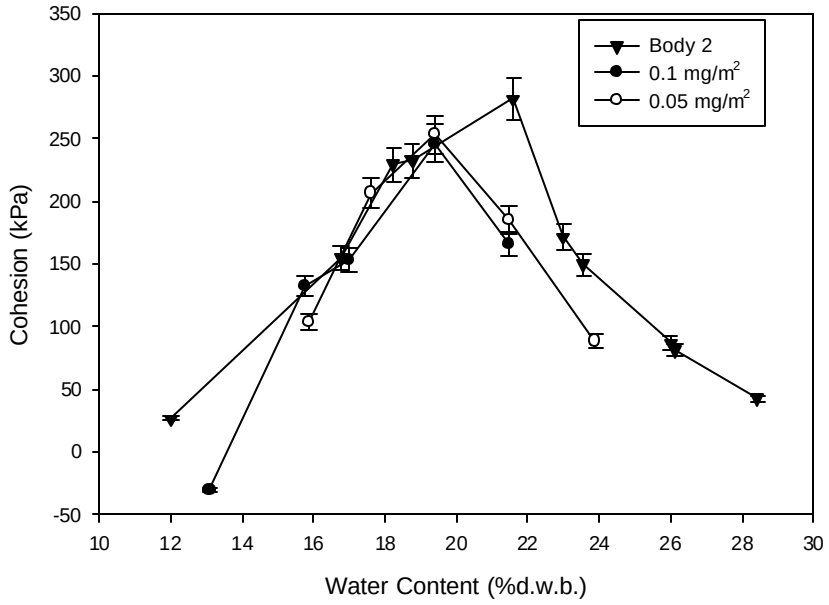

Figure 35. Cohesion versus water content for dispersant and $CaCl_2$ additions.

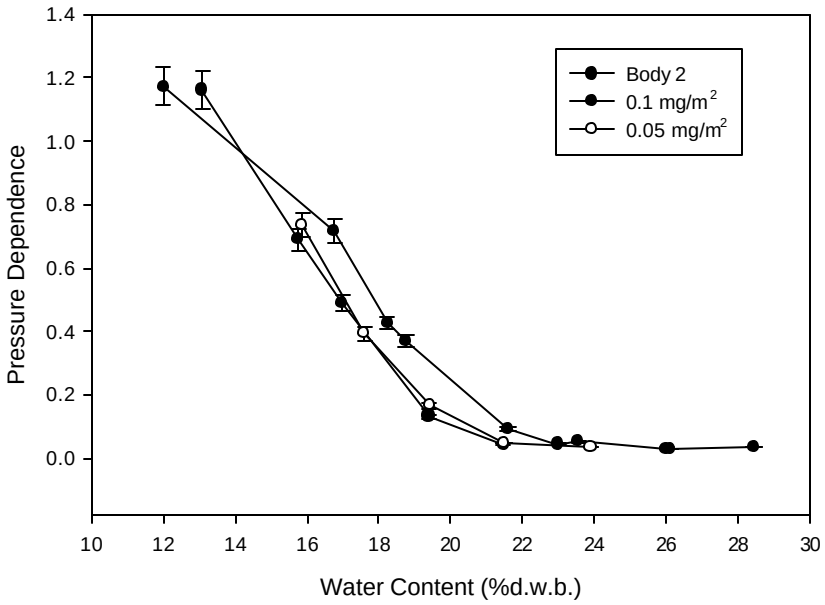

Figure 36. Pressure dependence versus water content for dispersant and $CaCl_2$ additions.

Flocculated and coagulated have different meanings, flocculated is used to refer to the condition in which particles are not as individual entities because of their original state, i.e. no complete dispersion has been accomplished. On the other hand, coagulated is used to refer to the condition of the system in which salts are added on purpose to promote agglomeration.

Packing differences that may arise between the flocculated and the coagulated state are believed to be responsible for the shift to lower water content levels of the curve with 0.05 mg/m^2 dispersant and $CaCl_2$ with respect to the original flocculated curve.

These plasticity plots can be used to estimate the water required for extrusion. Based on the previously determined extrudable range, the water content at 71 kPa was used to determine the water content necessary to produce an ideally extrudable body. For some plots, it was necessary to extrapolate the line. To do so, the same shape of the other plots was assumed. This is shown in Figure 37 and Figure 38. For the samples without $CaCl_2$, the results were 20.4 and 23.4 %d.w.b. for dispersant levels of 0.1 and 0.05 mg/m^2 respectively. For the samples with $CaCl_2$, the results were 24.1 and 24.7 %d.w.b. for dispersant levels of 0.1 and 0.05 mg/m^2 respectively. Compared to the original water content for extrusion of this body (27 %d.w.b.), a reduction is evident, moving this body towards water levels for extrusion more consistent with bodies 1 and 3. This would reduce the shrinkage of this body without altering fired properties[1].

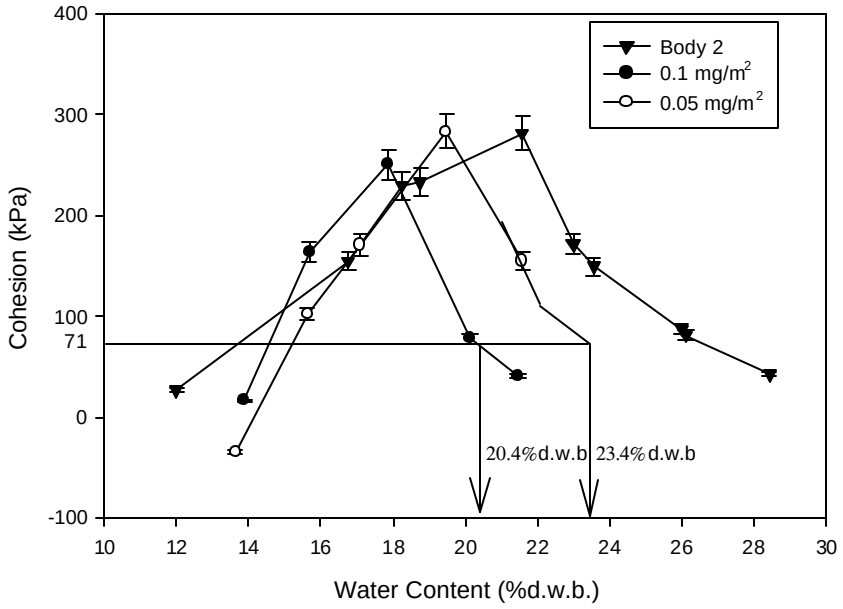

Figure 37. Estimation of water for extrusion for the samples with no $CaCl_2$.

[1] Properties of samples batched with 0.05 mg/m^2 of dispersant and $CaCl_2$ are presented in Appendix B.

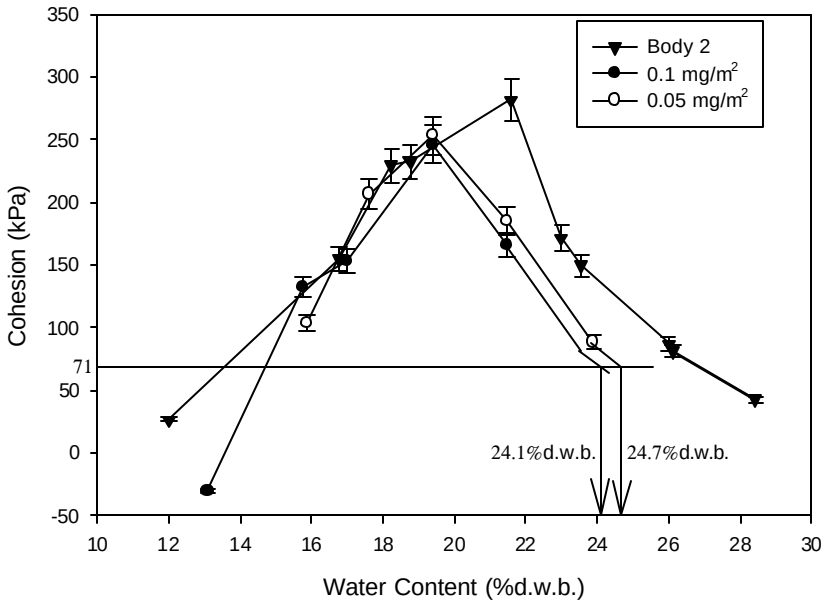

Figure 38. Estimation of water for extrusion for the samples with $CaCl_2$.

IV. CONCLUSIONS

The fired body under study was not significantly different from the reference bodies. Green and fired properties of the three bodies were similar. The body under study was better than the other bodies in terms of flexural strength and firing range, however, it was a less plastic body compared to the reference bodies. The difference in plasticity can be interpreted as requiring a higher water content to develop similar plastic characteristics.

The practical consequences of higher water requirement for extrusion are significant. More energy and time are required for drying. Higher shrinkage increases the chances of cracking during drying and firing, so drying and firing control and handling of the ware become critical.

The HPASC proved to be an excellent tool for the characterization of plasticity. It made possible the determination of differences in plastic behavior at conditions that resemble real processes. In spite of being a very simple method, the plastic limit was able to show differences in the plastic behavior of the bodies.

For this body, at the conditions tested, particle size distribution of the coarser fraction showed no effect on plasticity.

It was shown that plasticity can be manipulated by dispersant and coagulant additions. Reductions in the water content required for extrusion from 27 %d.w.b. to as low as 20.4 %d.w.b could be accomplished by additions of dispersant. Other aspects should be taken into account when choosing a level of dispersant or coagulant to improve plasticity. A coagulated system is preferred over a dispersed system because it is faster to filterpress, and it is less susceptible to dilatancy in high pressure processes like extrusion.

REFERENCES

1. W.M. Carty and U. Senapati, "Porcelain-Raw Materials, Processing, Phase Evolution, and Mechanical Behavior," *J. Am. Ceram. Soc.,* **81** [1] 3-20 (1998).

2. W.M. Carty, "Colloidal Nature of Kaolinite," *Am. Ceram. Soc. Bull.,* **78** [8] 72-6 (1999).

3. H.H. Murray and W.D. Keller, "Kaolins, Kaolins, and Kaolins," pp. 1-24 in *Kaolin Genesis and Utilization.* Edited by H. Murray, W. Bundy, and C. Harvey. Clay Minerals Society, Boulder, CO, 1993.

4. W.M. Carty, "Rheology and Plasticity for Ceramic Processing," *Ceram. Trans.,* **125**, 29-52 (1999).

5. F.H. Norton, *Fine Ceramics,* 2nd ed.*;* pp. 104-5. Robert E. Krieger Publishing, Malabar, FL, 1978.

6. W.M. Carty and K.R. Rossington, "Effects of Ionic Concentration on the Viscosity of Clay-Based Suspensions," pp. 199-211 in *Science of Whitewares 2.* Edited by W. M. Carty and C. W. Sinton. American Ceramic Society, Westerville, OH, 2000.

7. W.M. Carty, K.R. Rossington, and D.S. Schuckers, "Plasticity Revisited," pp. 225-36 in *Science of Whitewares 2.* Edited by W. M. Carty and C. W. Sinton. American Ceramic Society, Westerville, OH, 2000.

8. K.R. Rossington, "Colloidal Behavior of Clay in Whiteware Suspensions"; Ph.D. Thesis. Alfred University, Alfred, NY, 1999.

9. P. Sillapachai, "Effects of Processing Route on Aging"; M.S. Thesis. Alfred University, Alfred, NY, 2001.

10. J.E. Funk and D.R. Dinger, *Predictive Process Control of Crowded Particulate Suspensions Applied to Ceramic Manufacturing;* pp. 232-52. Kluwer Academic, Boston, MA, 1994.

11. W.M. Carty and C. Lee, "The Characterization of Plasticity," pp. 89-101 in *Science of Whitewares.* Edited by V. E. Henkes, G. Y. Onoda, and W. M. Carty. American Ceramic Society, Westerville, OH, 1996.

12. B. Baran, T. Erturk, Y. Sarikaya, and T. Alemdaroglu, "Workability Test Method for Metals Applied to Examine a Workability Measure (Plastic Limit) for Clays," *Appl. Clay Sci.,* **20** [1-2] 53-63 (2001).

13. G.Y. Onoda, "Mechanism of Plasticity in Clay-Water Systems," pp. 79-88 in *Science of Whitewares.* Edited by V. E. Henkes, G. Y. Onoda, and W. M. Carty. American Ceramic Society, Westerville, OH, 1996.

14. C. Hahn, "Variations in Raw Material Properties and How They Affect the Final Product, E.G. Porcelain," *Ceram. Forum Int.*, **60** [4] 144-9 (1983).

15. C.M. Caughel, "The Correlation of Clay Mineralogy with Suspension Rheology"; B.S. Thesis. Alfred University, Alfred, NY, 2000.

16. "Standard Test Methods for Chemical Analysis of Ceramic Whiteware Clays," ASTM Designation C 323-56 (Reapproved 1999). American Society for Testing and Materials, West Conshohocken, PA.

17. "Standard Test Methods for Apparent Porosity, Water Absorption, Apparent Specific Gravity, and Bulk Density of Burned Refractory Brick and Shapes by Boiling Water," ASTM Designation C 20-00. American Society for Testing and Materials, West Conshohocken, PA.

18. B.M. Pinto, "Effect of Filler Particle Size on Porcelain Strength"; M.S Thesis. Alfred University, Alfred, NY, 2001.

19. P.T. Kupinski, "The Effects of Water Chemistry on Clay-Based Suspension and Plastic Body Rheology"; M.S. Thesis. Alfred University, Alfred, NY, 2000.

20. J.D. McCann, "Effects of Mixing on Pyroplastic Deformation"; B.S. Thesis. Alfred University, Alfred, NY, 2004.

21. "Standard Test Methods for Liquid Limit, Plastic Limit, and Plasticity Index of Soils," ASTM Designation D 4318-00. American Society for Testing and Materials, West Conshohocken, PA.

22. H. Lee, Alfred University, Alfred, NY, November, 2004, Private Communication.

23. W.M. Carty, Alfred University, Alfred, NY, November, 2004, Private Communication.

APPENDIX A. Characterization of Raw Materials

In order to gain better understanding of the characteristics and behavior during processing of the body under study, the raw materials used for its manufacturing were characterized.

1. General Properties

Table X. Density, SSA, and LOI of the Raw Materials.

RAW MATERIAL	DENSITY (g/cm^3)	SPECIFIC SURFACE AREA (m^2/g)	LOI (%)
Feldspar LD	2.61	2.85	0.6
Quartz OL	2.64	3.33	1.5
Ball Clay SF	2.63	32.65	12.4
Ball Clay LI	2.73	14.21	5.4
Ball Clay MA	2.55	37.30	12.1
Kaolin AR	2.60	25.37	14.0
Fired Scrap	2.54	1.06	0.3

2. Chemical Analysis

Table XI. Chemical Composition of the Raw Materials.

RAW MATERIAL	Feldspar LD	Quartz OL	Ball Clay SF	Ball Clay LI	Ball Clay MA	Kaolin AR	Fired Scrap
SiO_2 (wt%)	77.55	95.4	57.49	64.38	71.03	54.19	71.19
Al_2O_3 (wt%)	13.64	4.03	36.03	26.96	24.82	42.71	22
Fe_2O_3 (wt%)	0.24	0.3	2.42	1.11	1.8	1.71	0.93
MgO (wt%)	0.05	0.02	0.45	0.46	0.37	0.2	0.23
CaO (wt%)	0.39	0.02	0.19	0.02	0.13	0.06	0.43
Na_2O (wt%)	3.28	<0.01	0.08	0.67	0.05	0.06	1.44
K_2O (wt%)	4.75	0.09	0.7	4.76	0.56	0.32	2.85
TiO_2 (wt%)	0.06	0.12	2.44	1.47	1.04	0.7	0.7
P_2O_5 (wt%)	<0.01	<0.01	<0.01	<0.01	0.07	<0.01	<0.01
MnO (wt%)	0.01	<0.01	0.02	<0.01	<0.01	<0.01	0.01
Cr_2O_3 (wt%)	0.00	<0.001	0.07	0.01	0.01	0.00	0.02
Traces* (wt%)	0.02	0.00	0.1	0.12	0.09	0.02	0.15
* Traces include: Ba, Ni, Sr, Zr, Y Nb, and Sc							

3. Particle Size Distribution (PSD)

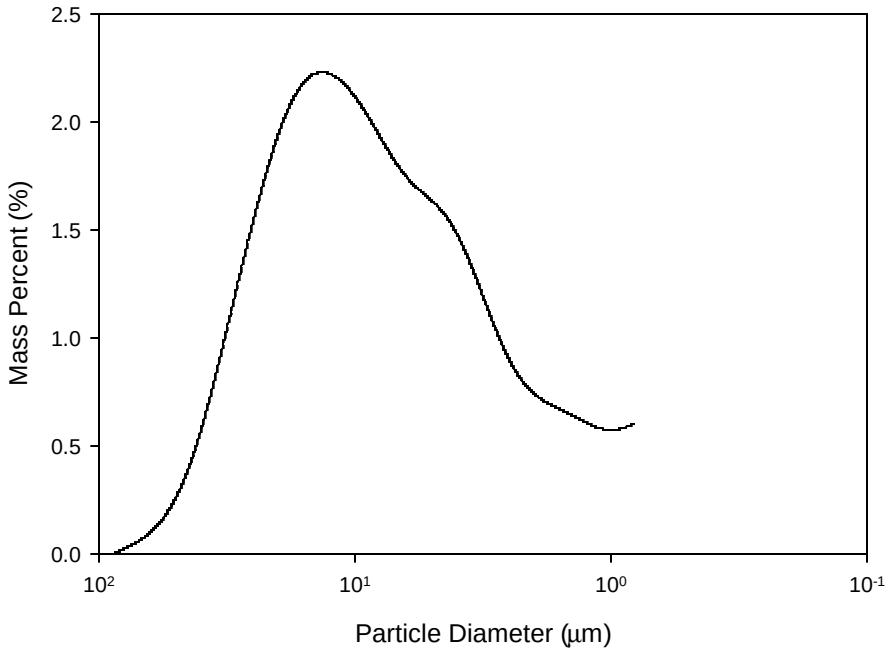

Figure 39. Particle size distribution of feldspar LD.

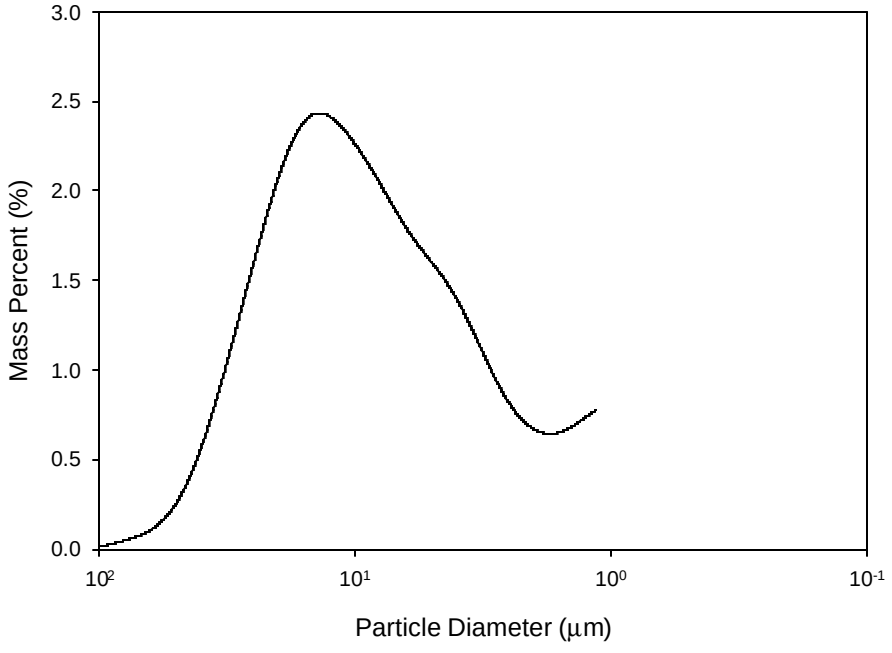

Figure 40. Particle size distribution of quartz OL.

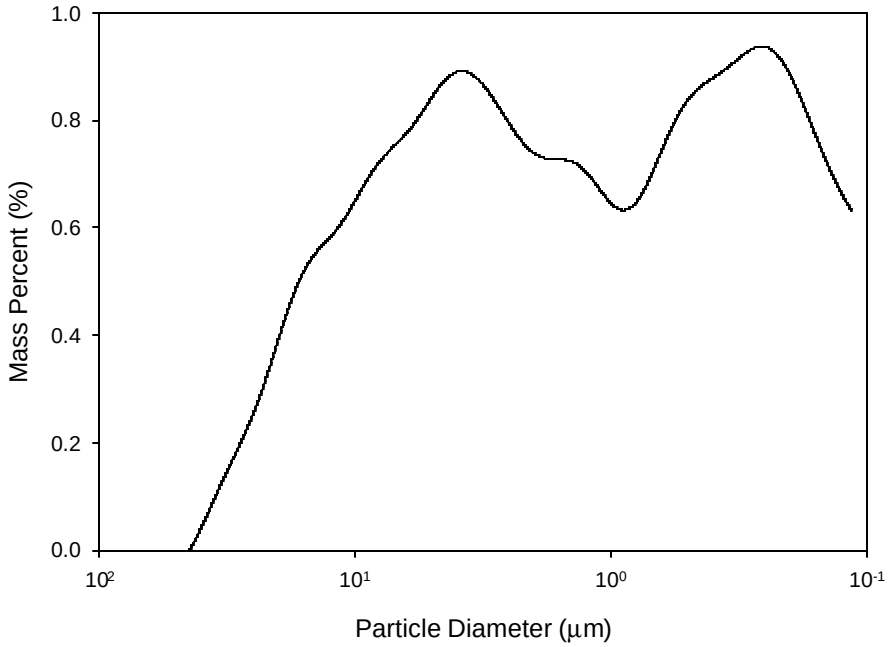

Figure 41. Particle size distribution of ball clay SF.

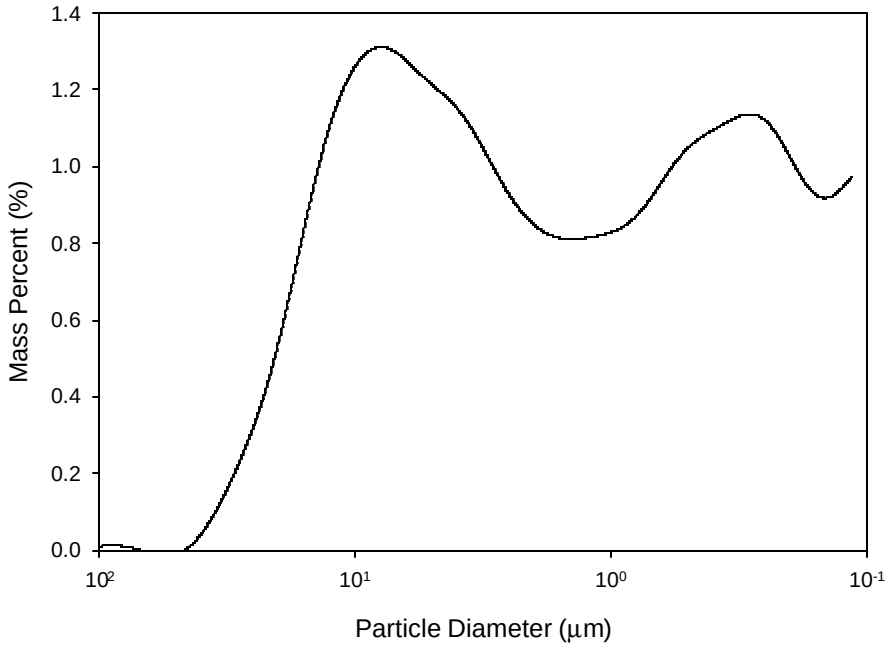

Figure 42. Particle size distribution of ball clay LI.

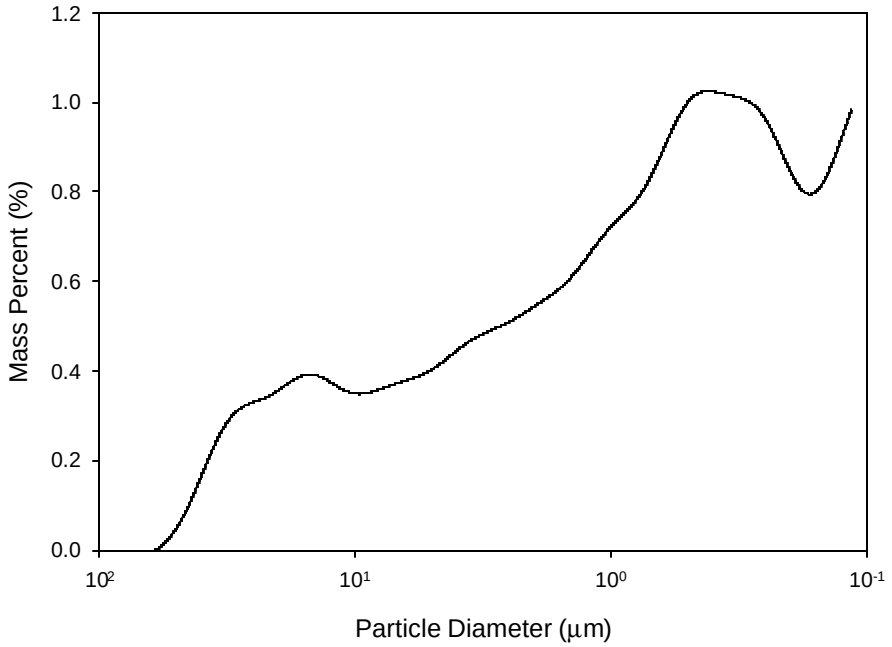

Figure 43. Particle size distribution of ball clay MA.

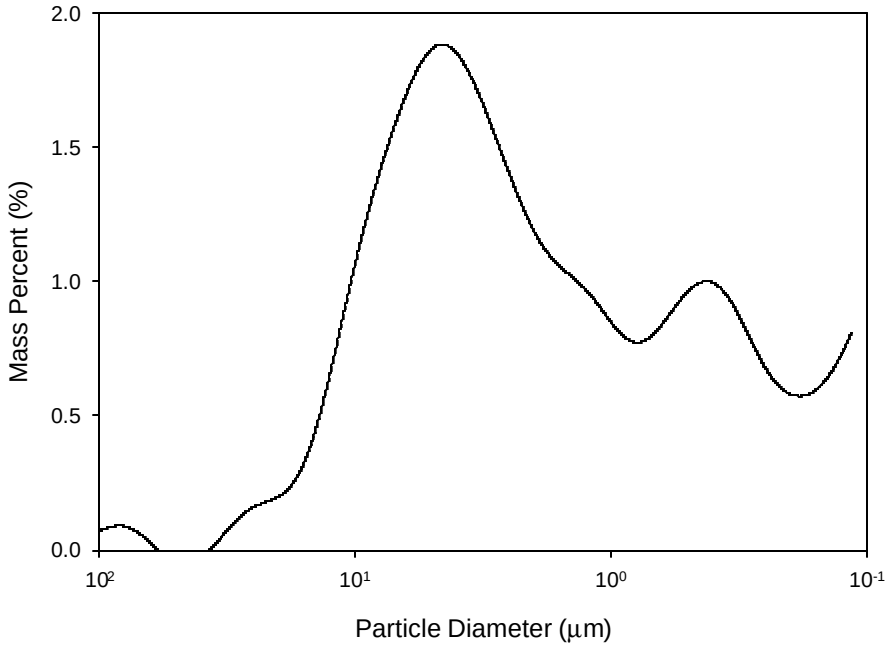

Figure 44. Particle size distribution of kaolin AR.

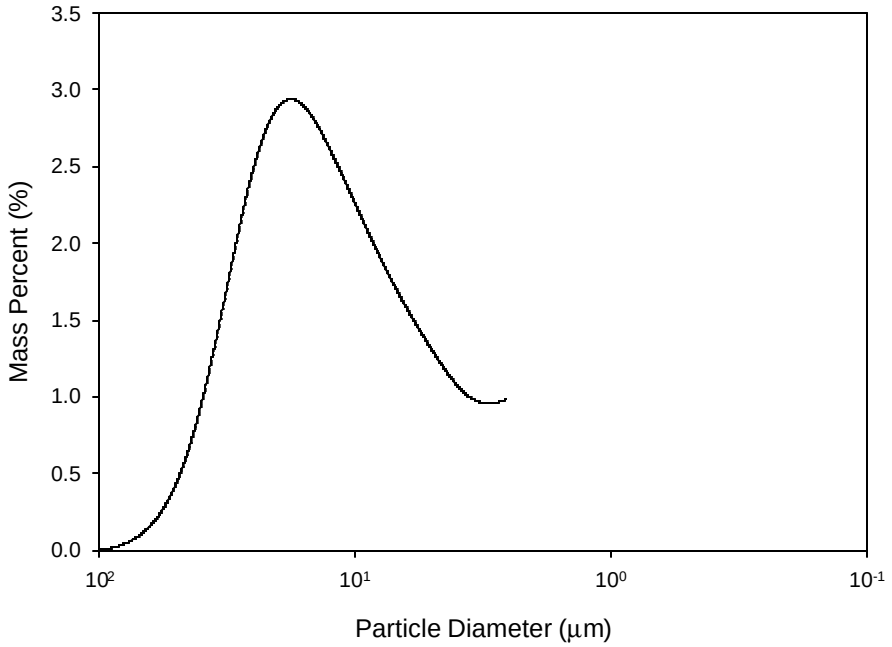

Figure 45. Particle size distribution of fired scrap.

APPENDIX B. Properties of the Body under Study with Modified Plasticity

A sample of Body 2 was batched with 0.05 mg/m^2 of Darvan 811. Before dewatering, calcium chloride was added to reach a 10 mM [Ca^{+2}]. The sample was extruded, dried, and fired in the same way as the samples for the comparison of fired properties. Drying and firing shrinkage was measured by scribing marks 100 mm apart on the rods and measuring that distance after drying and firing. The firing temperature was 1289°C.

Water content during extrusion and shrinkage are shown in Table XII. Fired properties are shown in Figures 46 to 48. It can be seen that modifying the plasticity of the body by dispersant and coagulant additions allowed the body to be extruded at lower water content, reducing drying and firing shrinkage without affecting the fired properties.

Table XII. Water Content During Extrusion and Shrinkage of Body 2 with Modified Plasticity Compared with the Other Bodies.

Body	**Water Content for Extrusion (% d.w.b.)**	**Drying Shrinkage (%)**	**Firing Shrinkage (%)**
1	20	4.3 ± 0.1	6.8 ± 0.1
2	27	6.0 ± 0.4	7.1 ± 0.2
2 with modified plasticity	25	5.1 ± 0.3	6.7 ± 0.2
3	21	4.9 ± 0.2	6.1 ± 0.2

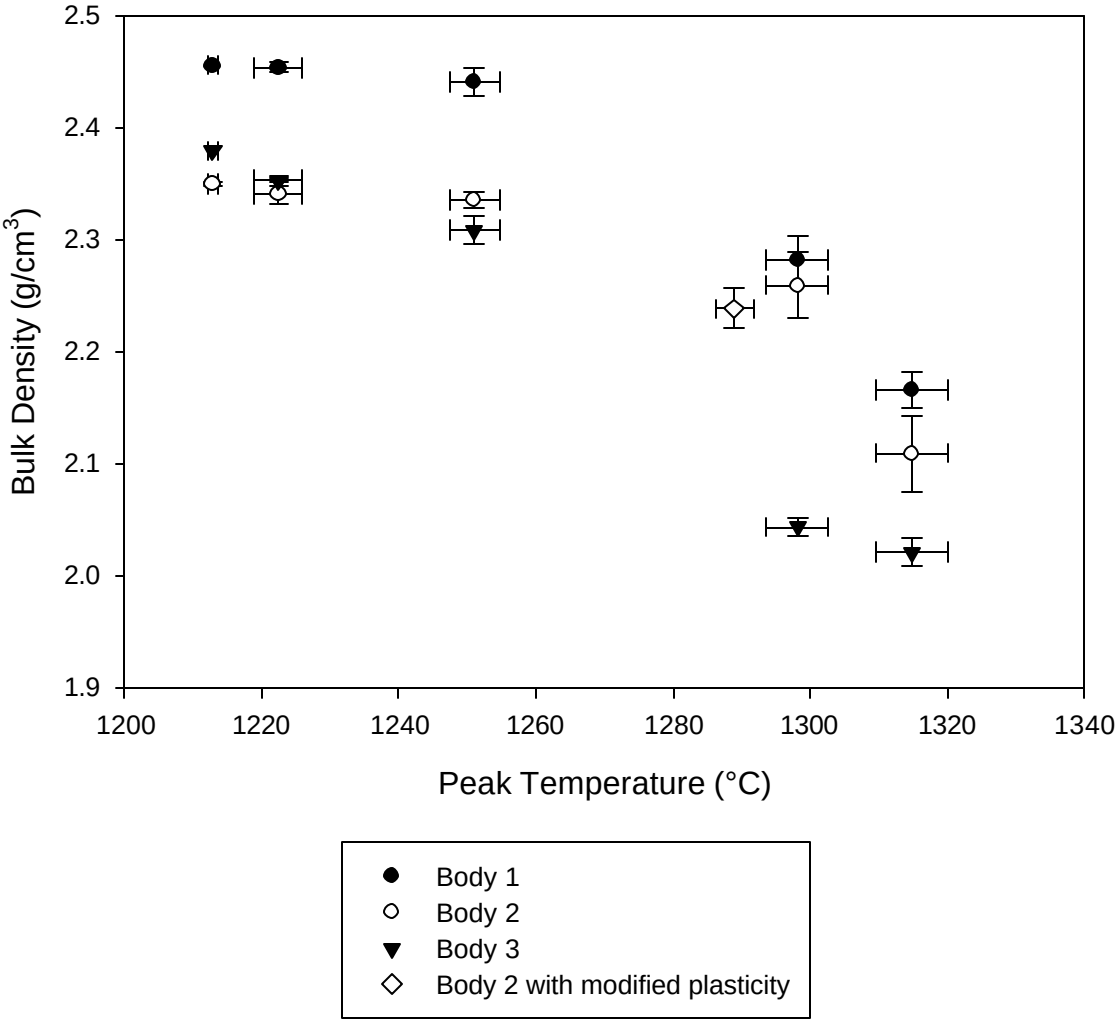

Figure 46. Bulk density of Body 2 with modified plasticity compared with the other bodies.

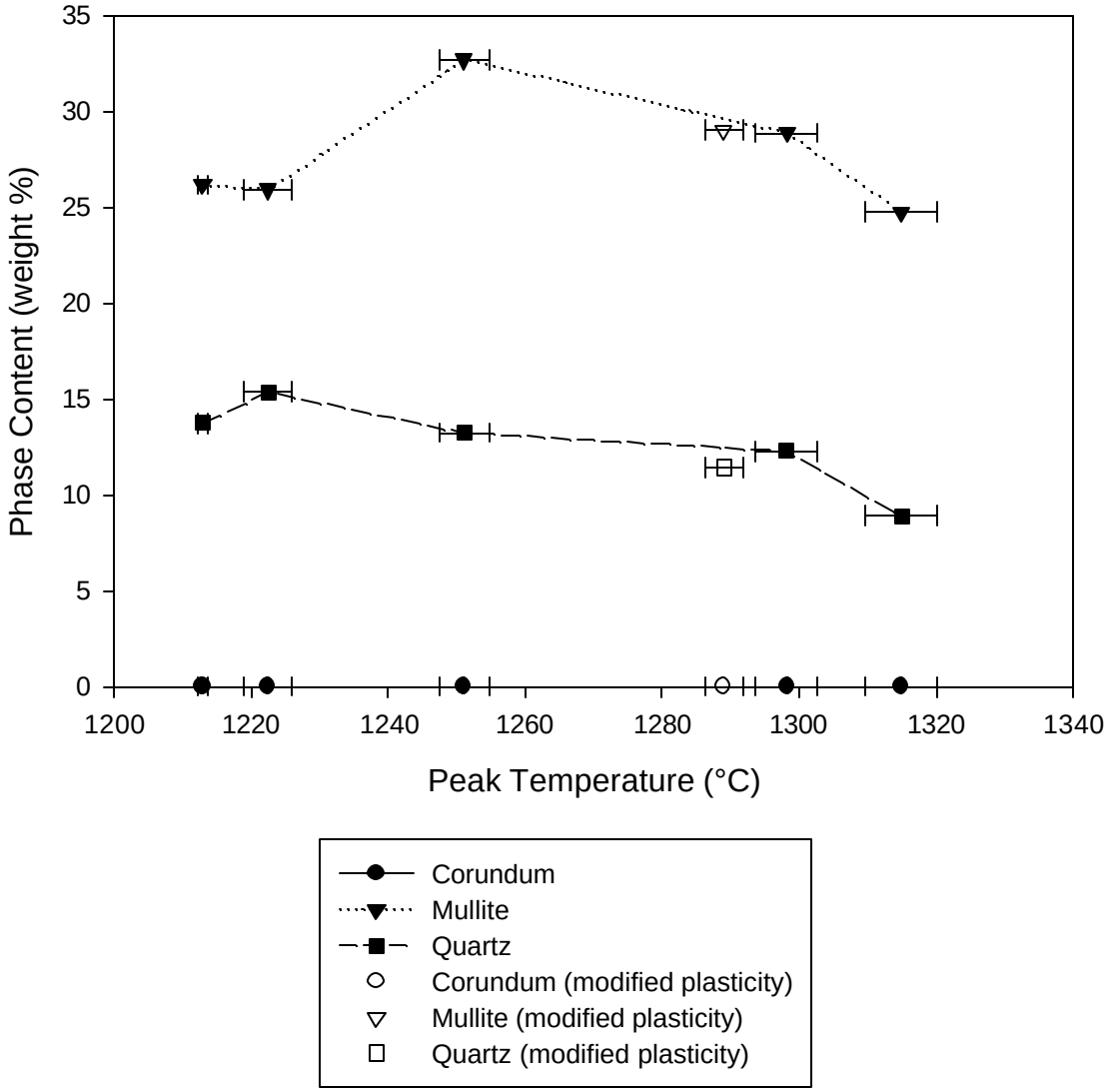

Figure 47. Concentration of crystalline phases in Body 2 with modified plasticity compared with regular Body 2.

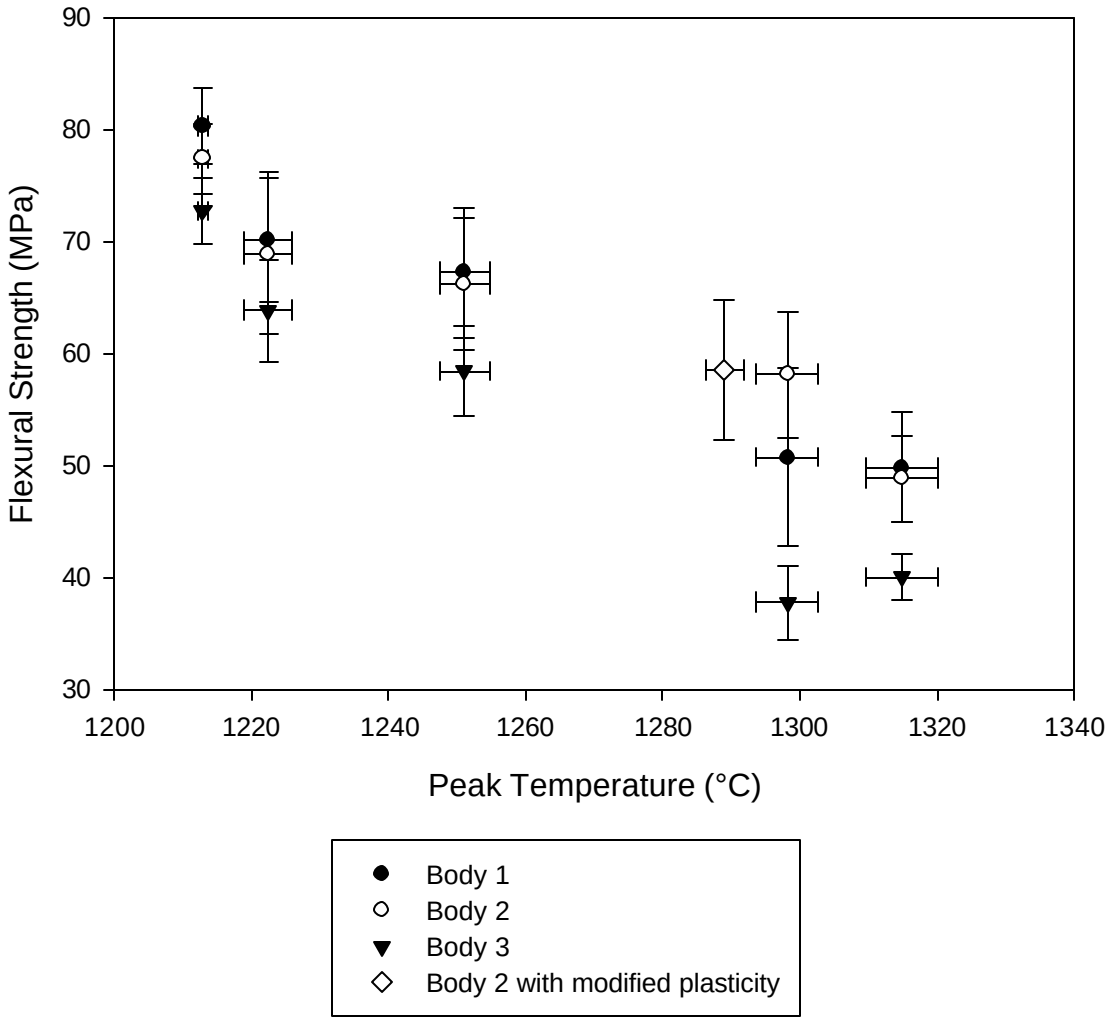

Figure 48. Flexural strength of Body 2 with modified plasticity compared with the other bodies.

APPENDIX C. Location of the Bodies in the Phase Diagram

The chemical composition of the bodies was used to locate them on the Silica-Leucite-Mullite sub-diagram, shown in

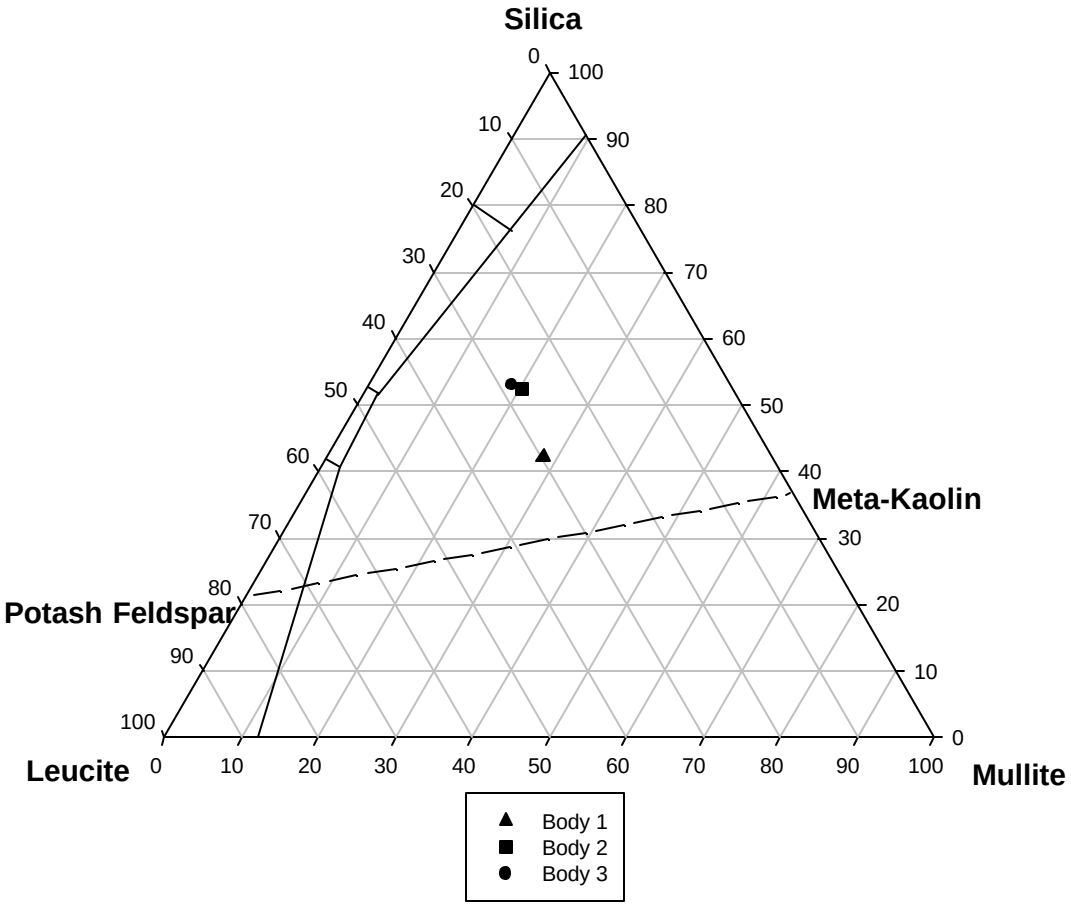

Figure 49. Location of the bodies in the phase diagram.